Mass spectrum of proton-proton inelastic interactions from 55 to 400 GeV/c at small momentum transfer

R. D. Schamberger, Jr., J. Lee-Franzini, R. McCarthy
State University of New York at Stony Brook, Stony Brook, New York 11794

S. Childress and P. Franzini
Columbia University, New York, New York 10027

(Received 28 January 1977; revised manuscript received 21 November 1977)

The doubly differential cross section $d^2\sigma/dtdM^2$ for the reaction $p+p\to p+X$ was measured as a function of the four-momentum transfer squared (t), the missing-mass squared (M^2), and the total center-of-mass energy squared (s). We covered the region $0.024<-t<0.234$ (GeV/c)^2, $0<M^2<0.12\,s$, and $105<s<752$ GeV^2, by detecting the slow recoil proton at large angles with solid-state detectors. The data were taken on polypropelene $[(CH_2)_n]$ and carbon targets, and a subtraction was made to obtain the free-proton cross section. We find that our differential cross section can be simply represented by $d\sigma(s)/dM^2=[(15\pm0.5)/s+(2.9\pm0.1)/M^{3.7\pm0.1}]$ mb/GeV^2. If the energy-independent part of this result is identified with the inelastic diffractive process then we obtain $\sigma_{\rm diff}=3.6\pm0.4$ mb after doubling for p-p symmetry. We also observe no significant increase with s for the inclusive cross section integrated to $0.06s$ or $0.1s$.

I. INTRODUCTION

The inclusive reaction $p+p\to p+X$ was studied versus energy at the internal target area (ITA) of Fermilab by interacting the proton beam during both the accelerating cycle and the coasting time, on polypropene $[(CH_2)_n]$ and carbon fibers, and obtaining the free-proton cross section by subtraction. For an inclusive reaction, only three kinematical variables need to be defined. One variable, the total energy squared in the center of mass s was known by a knowledge of the magnetic field in the main-ring magnets (to ±1%). The other two variables were defined by measuring in the laboratory the kinetic energy T and scattering angle θ of each detected slow-recoil proton. From these variables, the usual Lorentz-invariant variables M^2, the total energy squared of X in its center of mass, and t the four-momentum transfer squared from the target to the recoil proton, can be calculated. We therefore measure the doubly differential yield $d^2N/dtdM^2$, which with appropriate normalization results in absolute measurements of the inelastic cross sections $d\sigma/dtdM^2$.

The cross sections $d\sigma/dtdM^2$ were measured over the range in t and M^2 of $0.024<|t|<0.234$ (Gev/c)^2, $M^2<0.12\,s$, at seven average s values from 114 to 741 GeV^2, corresponding to laboratory beam momenta P from 55 to 400 GeV/c.

This study was partly motivated by the following questions:

(1) *Diffraction dissociation.* The possibilty of observing diffractive inelastic processes producing states X of large mass was first pointed out by Good and Walker in 1960.[1] We are interested here in determining whether this process can be unambiguously separated from the general inelastic cross section by identifying a contribution to the inelastic cross section which is energy independent. Another important property of the inelastic diffraction is the shape of the mass spectrum for which some models make explicit predictions.[2]

(2) *Rising total cross section.* This phenomenon, observed at both CERN ISR[3] and Fermilab,[4] is still in need of an explanation. Both theoretical[5] and experimental[6] claims have been made to the effect that this rise is all due to a rise of the inelastic diffractive cross section. This would imply that the diffractive cross section should rise by over 1 mb over our energy range.[7]

(3) *Scaling contribution to the inclusive cross section.* There is considerable interest[8] in the magnitude as well as the M^2 dependence of a Feynman-scaling contribution to the inclusive cross section.

(4) *The relative magnitudes of the elastic, diffractive, and total cross sections.* In 1973, Pumplin[9] derived a unitarity bound limiting the diffractive cross section to be less than $\frac{1}{2}$ of the total cross section minus the elastic cross section. This experiment measures simultaneously the elastic and diffractive cross section, yielding information on how saturated is the Pumplin bound.

Our results can be summarized as follows:

(a) The inclusive cross section, integrated over t and up to a constant fraction of available phase

space in M^2 (i.e., up to a constant fraction of s) is independent of s to a few percent. A typical value is $\sigma_{\text{inc}}(M^2 < 0.1s) = 3.3$ mb.

(b) The measured inclusive cross section integrated over our t range appears to be composed of two terms, the first term is energy independent, i.e., $(d\sigma/dM^2)_{\text{I}} \sim f(M^2)$ and the second term scales with energy, i.e., $(d\sigma/dM^2)_{\text{II}} \sim (s^{-1})g(M^2)$.

(c) Specifically, all our data are well represented by the empirical formula $d\sigma/dM^2 = (15/s + 2.9/M^{3.7})$ mb/GeV^2, with s and M^2 both measured in GeV^2. From this we conclude that we can identify an approximately energy-independent contribution to the inclusive cross section given by $(d\sigma/dM^2)_{\text{energy-independent}} = [(2.9 \pm 0.1)/M^{3.7 \pm 0.1}]$ mb/GeV^2. The integral of this cross section has no logarithmic rise with s and is given over our s range by 1.8 mb. Because of the symmetry of the initial p-p state, the total energy-independent contribution to the inelastic cross section is twice the above value or, $\sigma_{\text{energy-independent}} = 3.6 \pm 0.4$ mb for $262 \leq s \leq 741$ GeV^2.

(d) If we assume this energy-independent contribution to be due to inelastic diffraction (which on geometrical grounds is expected to be energy independent), we note that our value for $\sigma_{\text{diffractive}}$ is much smaller than the currently accepted value of 6 to 9 mb. These values are in fact the total cross section for $pp \to pX$ with $M^2 \lesssim 0.1\,s$ and they include large contributions which scale with s (our value for this cross section is 6.6 mb). We believe that by identifying the energy-independent part of $\sigma(pp \to pX)$ we have separated out the diffractive component of the inclusive cross section. We note that its magnitude of 3.6 mb is far from saturating the unitarity bound[9] $\sigma_{\text{inelas. diff.}} < 13$ mb.

(e) Our data are poorly described by the triple-Regge[10] formalism and we observe no contribution from a triple-Pomeron coupling to $\sigma(pp \to pX)$ in our s, t, and M^2 region.

(f) We have no disagreement over measured quantities with other experiments performed in the past to determine inelastic diffraction. We disagree with the inferences drawn by other authors.

II. EXPERIMENTAL METHOD

A. Introduction

Very-high-energy inclusive scattering is much more precisely investigated by detecting the slow recoil proton rather than the fast forward particle because (a) there is enormous amplification in the range of the scattering angle, (b) the momentum transfer is directly the recoil momentum, rather than a minute fraction of the forward particle's momentum. This method presents its own problems. Specifically since most of the cross section is for $|t| < 0.2$ (GeV/c)^2 and $t = -2mT$, where m is the proton mass and T its kinetic energy, one has to detect and measure protons with $T < 100$ MeV. While these energies are unusual in high-energy physics, they are in fact very accurately measurable with proper techniques and precautions. For energies around 10 MeV, multiple scattering can become large and the proton range is only about 0.1 g/cm^2. Thus the target thickness must be kept well below such values, i.e., should be $\approx$0.01 g/cm^2. In addition, for the scattering angles of interest (45° to 90°), it is in practice difficult to cover large solid angles. Both these two constraints result in the necessity of very intense beams. In particular, to achieve reasonable data rates ($>10^3$ events/machine cycle), at least 10^{12} protons/sec on target are necessary. We ran a preliminary phase of this experiment in the external proton beam at Fermilab in the neutrino area.[11-15] Because of our interest in the energy dependence of the inclusive cross sections, the present experiment was performed at the ITA of Fermilab. Since the protons go around the main ring 50 000 times/sec, a typical accelerator intensity of 6×10^{12} protons per pulse corresponds to an on target intensity of 3×10^{17} protons/sec.

B. Target

This very high intensity is best matched by a target density of $\sim 10^{-7}$ g/cm^2. We used a target of about sixty 20-μ $(CH_2)_n$ fibers and sixty 8-μ carbon fibers mounted on a wheel rotating at 65 rps. Hence these fibers had effective thicknesses of $\sim 1.2 \times 10^{-5}$ g/cm^2. The appropriate interaction rate was achieved by inserting the fiber tips in the dense fringe of the beam from below (see Fig. 1). The main concern with the (CH_2) fibers was to prevent excess beam exposure which could produce heating and melting, resulting in enlarged tips of these fibers. In addition, the target had to be removed at injection so as not to produce large beam losses at low beam energy, and then rapidly inserted and kept in the beam for 1 sec for each cycle. Finally, the beam shrinks in size during acceleration, has various slow oscillations, and sometimes sudden increases in vertical size during a cycle. For all three reasons the height of the target was continually adjusted by a closed-loop servomechanism which kept the interaction rate constant to within 20%. An optical synchronization signal told our data-collection system which target was in the beam and all nuclear-fragments production from each were con-

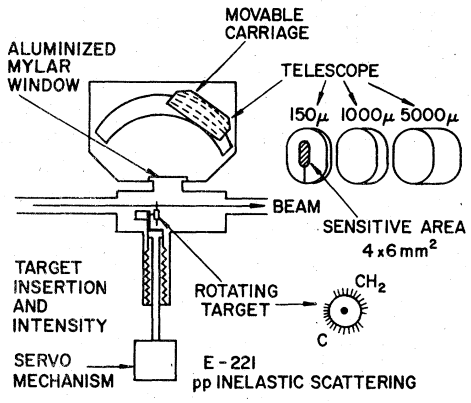

FIG. 1. A schematic diagram of our experimental setup.

stantly scaled. Target-out versus target-in rates were less than 0.1%, of which less than 1% would be candidates as acceptable events.

C. Proton-recoil detectors

The proton recoils were detected by nine solid-state detector telescopes. Eight were mounted on a movable carriage with a fixed angular separation of 2.406°. This carriage was mounted on a fixed arc centered around the target and by using a stepping motor and an absolute optical encoder, we could remotely position it in the range of 50° to 130° with a reproducibility of 0.01° and an accuracy of ±0.05°. All these telescopes could be moved beyond 90°. One telescope was mounted at a fixed angle (83°) which is approximately the peak in the laboratory of p-p elastic cross sections. The fixed-angle telescope monitored the (beam)×(hydrogen-in-target) luminosity by counting elastic recoils. The number of elastic protons per run in this fixed-angle monitor provided relative normalization between runs.

A telescope consisted of three detectors, each a 1-cm² totally depleted silicon-surface-barrier solid-state detector (D_0,D_1,D_2). Their respective thicknesses were 150±15, 1000±10, and 5000±50 microns. The first detector was only used to define the acceptance of the telescope and not used in the energy determination. For this purpose, special detectors with charge-collection electrodes deposited over only a small fraction of the active area were used (see Fig. 1). The electrode was deposited over a rectangular area 4×6 mm². Since the 4×6-mm² active area was sufficiently less than the size of the other two detectors, the edge effects for the thicker detectors which would impair resolution were eliminated. The edge effects of D_0 reflect themselves only in a 10% momentum dependence in the solid-angle acceptance which can easily be calibrated. The detectors rotated on an arc of radius 92 centimeters centered at the target subtending a solid angle of 2×10^{-6} sr per telescope with an acceptance in θ of ±0.125°. Calibration of the relative solid angle of each telescope was performed by positioning each telescope at an identical angular position and counting the number of elastic proton recoils per monitor proton. This information gives the relative normalization between telescopes. The whole detector-carriage system was enclosed in a vacuum chamber which was directly connected to the main ring. A 0.2 mil aluminized Mylar window reduced electromagnetic beam induced noise.

Since carbon nuclei were present in our targets, copious nuclear-fragment production (d,t,^{3}He,^{4}He...) was observed,[12] a fortuitous fact which rendered the application of the standard CH_2-C method elegantly accurate (see Sec. III A). The telescopes therefore performed the following functions: (a) produced a trigger, (b) identified particle type, (c) measured T, (d) measured θ. The telescopes are sketched in Fig. 1. The trigger was provided by a coincidence between D_0 and D_1. The particle identification was provided by detectors D_1 and D_2 for particles stopping in D_2. The identification was by means of the well-known method of using the correlation between the energy deposited signals E_1 and E_2, measured in the form of charge produced in the totally depleted Si crystal by the ionizing particle. The correlation for stopping p, d, and t is given by the upper branches of the respective curves in Figs. 2a and 2b. T is obtained as the sum of E_1 and E_2.

We note here that if we were to limit ourselves to protons which stop in D_2, we could only measure proton energies up to 35 MeV in our setup. Since the cost of the amount of Si necessary to stop 100 MeV or more protons is prohibitive, we have extended the method to higher-energy protons which fully cross D_2.[13] These latter protons have higher energy than the stopping protons, hence ionize less, causing the correlation curve to fold back as shown in Figs. 2a and 2b. Assuming the detected particle to be a proton, a good T measurement can be obtained from the measured E_2 value. The $T(E_2)$ relation can be derived from a knowledge of the range-energy relation for protons in Si and of the exact thickness of the detectors trivially to 1%. We preferred instead to obtain the $T(E_2)$ relation for each telescope empirically by placing it at known angles and observing the postion of the elastic peak whose recoil energy was calculated from kinematics. The relative $T(E_2)$ relations between these almost identical telescopes were determined to $\frac{1}{4}$%. The E_1 vs E_2 plots were displayed online during data

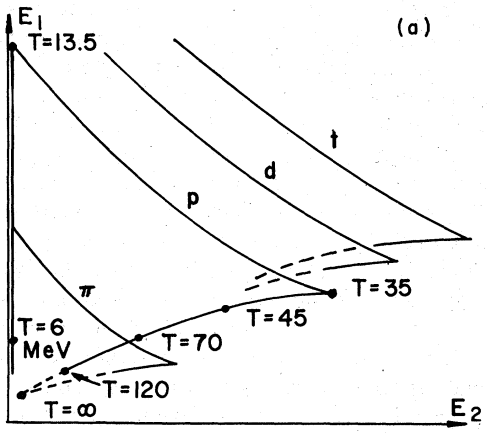

FIG. 2. (a) The theoretical range-energy correlation curve for four particles (pions, protons, deuterons, and tritons) in our experimental apparatus.

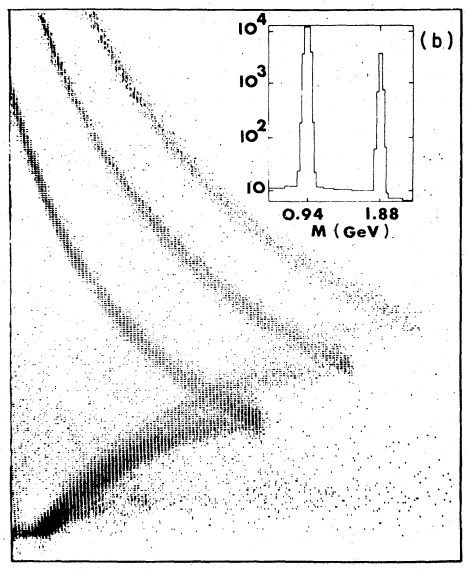

FIG. 2. (b) Scatter plot of E_1 vs E_2 for $\sim 10^{16}$ recoil particles. π mesons are barely visible above background. The insert is a plot of the number of events vs mass of the particle showing our excellent particle separation and indicating the low accidental background levels.

taking as they are extremely sensitive monitors of running conditions. Any sudden change in the whole chain of data collection apparatus (including for example accelerator conditions) visibly alters the width, postion, density of points both on the correlations curves and over the whole E_1-E_2 domain. In particular, this also turned out to be a rather sensitive method of monitoring background since any source not at the postion of the target caused events to cross the telescope at rather large angles, destroying the range-energy correlation. Since most of these events are high-energy events, they tended to fill the minimum ionizing corner of the plot. However, the correlation curve for pions is located near the minimum ionizing point (see Fig. 2a). Since pions are not copiously produced at large angles in the laboratory, it is difficult to observe this correlation curve if even the slightest amount of background were present. All of our data were taken under conditions where the background was low enough to observe the pion curve (see Fig. 2b). Our kinetic energy range was from 12 to 120 MeV, with about 200 keV [full width at half maximum (FWHM)] energy resolution at low T and increasing to about 5 MeV at the highest T.

D. Electronics

All the electronics used were designed and constructed for the present experiment.[14] Solid-state detectors require charge-sensitive amplifiers with sensitivity of ~1 V/pC, noise ~ of 5×10^{-3} pC, to fully use the Si-detector energy resolution. To obtain reasonable resolving time, the rise time of the output signal from the charge-sensitive amplifiers (preamps) must be $\lesssim$50 nsec. We have designed preamps with these characteristics. Their typical rise time is ~20 nsec into a 50-Ω load. These preamps, moreover, operate in vacuum which added a constraint in design due to power dissipation considerations. The preamp itself was placed within 2 inches of the detector to minimize noise and rise time. The detector-preamp assembly was kept at 70 °F ± 5 °F by a heat exchanger; at such temperature and constancy, any gain change due to temperature variations was $<\frac{1}{4}\%$.

Since the experiment itself was underground in the main-ring tunnel and approximately 150 ft of cable was necessary to bring a signal to the electronics trailer, the preamp signals were fed to delay-line clipping linear amplifiers prior to their transmission through the long cables. The linear amplifiers have a gain of 10, rise time of ~50 nsec and clipping time of ~1 μsec. The combination of charge preamp and differentiating amplifier shows no loss of energy resolution for pileups resulting in a dc output from the preamps corresponding to 50 times the magnitude of single particle signals. The analog signals were fed to discriminators and to a second delay-line amplifier followed by a track and hold amplifier. One such channel was used for each detector.

A master trigger signal was produced upstairs as the OR of the D_0D_1 coincidence from all the telescopes. A flag was set also for each telescope

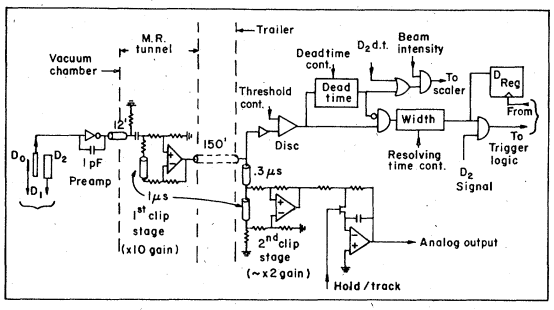

FIG. 3. Electronic channel for a telescope from detector to sample and hole, including discriminator and deadtime scalers.

giving a coincidence within 50 nsec of the master trigger (see Fig. 3). The master trigger switched, after an appropriate delay, all track and hold amplifiers to their hold mode. A small amount of transistor-transistor logic (TTL) was used to scan, upon receipt of a master trigger, all the flags. When an active telescope was found, the corresponding energy signals were switched through a set of silicon-on-sapphire metal-oxide-semiconductor switches from the track and hold amplifiers to two 12-bit successive-approximation analog-to-digital converters whose outputs were the E_1 and E_2 values in digital form (see Fig. 4). An event was thus defined by (a) the two 12-bit E_1 and E_2 numbers (which will yield T and particle type), (b) a 3-bit number identifying in which energy bin the event occurred (energy bins being typically 1% wide), which will yield $s = 2m(E_{\text{beam}} + m)$, (c) a 4-bit number identifying which telescope recorded the event (which will yield θ), (d) a bit identifying whether the $(CH_2)_n$ or the C target was in the beam during the event's occurence.

Whenever a single detector triggered its discriminator, an updating 2-μsec deadtime was generated. The OR of two deadtime signals from the two discriminators of each telescope was used to

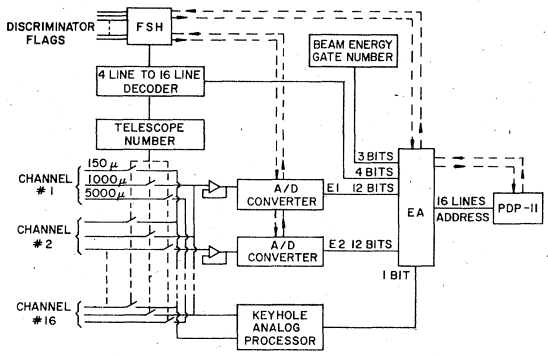

FIG. 4. Block diagram of flag scan, analog multiplexer and analog to digital conversion.

gate a scaler, for each telescope and energy gate, which counts a clock whose frequency was proportional to the instantaneous beam-on-target intensity. This gated count divided by the total clock count was a measure of the deadtime. The deadtime scalers counts were recorded for each carriage postion. Deadtimes were measured only for the $(CH_2)_n$ targets since their deadtimes were used to combine data from different telescopes after the free-hydrogen distributions had been obtained. Deadtimes were typically of the order of 1 to 7% varying monotonically with angle and they were measured to 1.5%.

E. Real-time analysis

During setup, tuning, and data taking in this experiment, well above 10^9 events as described above were taken. A minimum format for the above data would consist of two 16-bit words per event. Because of possible multiple events, 4 words were used. In the standard way of dealing with this information, one might fill a portion of the memory of a computer and write the memory content on tape whenever the memory was full. Three disadvantages were encountered with this method. First, the event rate was limited to the capacity of the buffer memory available. Second, a tape could only record a theoretical limit of 2.88×10^6 events. Third, the collected data must first be reduced to yield the information of particle type and T, etc., then a map of $d\sigma/dTd\Omega$ had to be produced. If this last step were performed on a reasonably large (i.e., 370/155) computer, we found that it required ~1 msec of central processing unit (CPU) time to fully dispose of an event. A small portion of our data, i.e., one tape or 0.3% of the data, would thus require approximately 1 hour of CPU time or typically a couple of days of calendar time to be reduced to a histogram of a physical cross section.

In a general-purpose computer, most of the time is spent in fetching instructions from core, obtaining and returning data to core, and in preparing input and output references. With the advances in solid-state technology in the late 1960's, it became clear to us that it should be possible to perform the complete event reduction with a specially built hard-wired computer in less than 1 μsec, a time scale small compared to the analog and digital operations described previously. The components needed for building such a special-purpose computer (2000 8-bit words of memory with 45 nsec read time, 16-bit adders with ≈40 nsec propagation time, 4×4-bit multipliers with 80 nsec execution time, various multiplexing, demultiplexing, and magnitude-comparison integra-

ted circuits were relatively inexpensive and available, such that an efficient program could be constructed with hardware with a gain in speed of a factor of a thousand and for a cost equivalent to executing the program 10^6–10^7 times on a general-purpose computer. This fact was borne out during the analysis of our two experiments.[13]

In detail, the special-purpose calculator (called here the event analyzer or EA) built for this experiment operates as follows: For every event E_1, E_2, telescope number, energy gate are input into the EA. Only E_1 and E_2 are actively used. The 12-bit E_2 word is divided into the 8 most significant bits called from now on E_2, and the 4 least significant bits called ΔE_2. E_2 addresses one of the 256 locations of 10 separate sets of memory of the appropriate number of bits. Figure 5 shows these memories and what is stored in each. For each value of E_2, the memory contains tables of the corresponding values of E_1 for protons, deuterons, and tritons as well as for protons crossing D_2. E_1 values are stored as 8-bit words. An acceptance width (W in Fig. 5) for each correlation is also stored. The main operation performed by the EA is the comparison of the measured E_1 value (truncated to 8 bits) with the stored E_1 value to identify particle type. For stopping protons, T is calculated by direct addition of the full precision E_1 and E_2 values. A different method is used to calculate T for particles crossing D_2. The function $T(E_2)$ and its derivative are stored in memory also. The first two terms in the Taylor expansion of T are calculated as shown in Fig. 5. If a particle is recognized as a nonstopping proton, it is this last value of T which is chosen. The four cases, crossing proton (proton down), stopping proton (proton up), deutron, and triton are checked sequentially in their most likely occurrence order. Figure 5 shows the memory outputs for the crossing-proton case. Note how four words are simultaneously output. Each path is linear and noniterative. The total propagation time for the crossing proton case is 156 nsec 95 nsec are necessary for each new case, giving an average analysis time of ~200 nsec. The EA end product is a T value which is packed together with telescope number, energy gate number, particle type, and target type to form a single 16-bit word. Finally, this word is used to address a location in a PDP-11 memory into which 1 is added. Since the addition was performed by the PDP-11, which used a stored program, this last step took some 10 μsec.

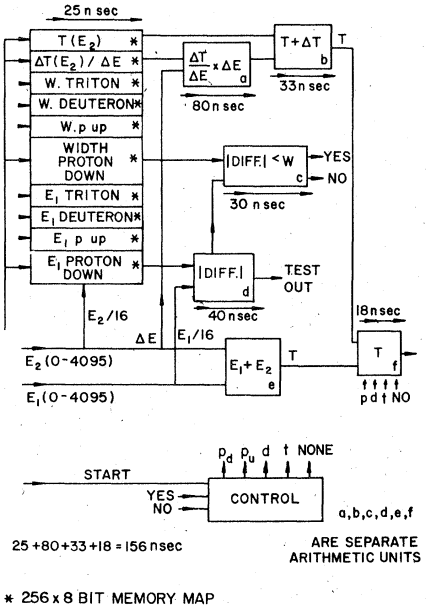

FIG. 5. Event-analyzer block diagram. The memory output for "proton down" case is shown. Each box is either a memory or an arithmetic unit as indicated. For a description, see text.

The result of the above described operations is a three-dimensional map in core of $d^2N(s)/dTd\Omega$. If 65 000 words of 16 bits each are available for storage, events can be accumulated until any one bin in the map should reach a count of 65 535. This would happen in our experiment every 10^8 events. At this point, the whole memory would have to be copied onto tape requiring ~160 inches of tape. In our case, since we had only 16 000 words of PDP-11 memory available, we addressed half words to increment their contents and were therefore limited to 255 counts per bin. Deuterons and tritons were recorded as total count (without T) and required an extra 1000 words of memory. The cross section was therefore written on tape for every 300 000 events using 40 in. of tape. Thus 10^9 events were contained in about four tapes as compared to 500 tapes. In fact, the histograms were dumped onto tape every 10 to 15 minutes (about $\frac{1}{2}$ million triggers) to minimize possible loss of data due to tape error or other possible failures. Note that 50% of the triggers had already been rejected. Most of these came from minimum ionizing particles whose energies were greater than 140 MeV.

Because of the event analyzer, we were able to process approximately 1 billion triggers in a short enough time to allow us to retake any data which were suspected of having background, thus eliminating the necessity of any correction for it. The background level in this experiment was reduced to 1/10 000 of the accepted events and this minute level was isotropic.

III. FINAL DATA REDUCTION

A. Free-H_2 cross section

From the three-dimensional maps of $d^2N(s)/dtd\Omega$ described above, the cross section in free H_2 can be obtained by subtracting run by run and telescope by telescope the carbon data with appropriate normalization from the polypropelene data. The proper normalization was obtained by counting deuterons and tritons produced in carbon and in polypropelene in each run, simultaneously with the counting of proton recoils in the identical telescope. Hence the ratio of these nuclear fragments from the two targets gave directly the correct ratio (effective beam intensity × carbon in target) with no correction necessary for beam-duty cycle and telescope deadtime.[12] Thus, despite the fact that free-proton interactions were approximately 10% of the total beam polypropelene interaction, the subtraction was performed with high precision (≈2 parts in 10^3). The measured individual deadtimes were applied to the subtracted free-H_2 distribution when combining different runs (≈3.5% on the average).

The free-H_2 $d^2N(s)/dTd\Omega$ was transformed bin by bin to $d^2N(s)/dtdM^2$ by computing the appropriate Jacobian. These distributions, when normalized appropriately by multiplying with a normalizing constant (see next section), yielded $d^2\sigma(s)/dtdM^2$, of which Fig. 6 is a typical plot: $d^2\sigma/dtdM^2$ vs M^2 for an s of 565 GeV and $0.023 < |t| < 0.080$ $(\mathrm{GeV}/c)^2$.

It is plotted on a log-log scale to demonstrate our extremely good mass-squared resolution and to show our total M^2 range. M^2 is expressed in terms of (T, θ) by

$$M^2 = m^2 + 2p_{\mathrm{beam}}p_{\mathrm{recoil}}\cos\theta - 2(E_{\mathrm{beam}} + m)T .$$

Our mass resolution is dominated by the angular resolution at low T (± 0.125°) yielding 1 GeV^2 (FWHM) at 300 GeV/c incident beam momentum. At high T, it is dominated by the kinetic-energy resolution and becomes 3 GeV^2 (FWHM).

B. Elastic- and inelastic-events separation

These cross sections contain both elastic and inelastic contributions (as seen in Fig. 6). The elastic and inelastic contributions to the data were trivially separable at low beam energy ($E_{\mathrm{beam}} \sim 50$ GeV) as the elastic peak was completely separated from the continuum. At such energies, one notes that the peak indeed has the expected shape of a Gaussian folded over the T interval equivalent to the angular acceptance of the detectors (see Fig. 7). Such a symmetric Gaussian shape persists even as the mass resolution broadens linearly with the increase in beam energy (as in all recoil-proton experiments) and the elastic peak merges with the inelastic continuum (see Fig. 6). In all cases, the elastic peak falls for $M^2 < m^2$ by more than three orders of magnitude and is well below the inelastic signal.

While we can separate elastic and inelastic contributions in the $d^2N(s)/dtdM^2$ histograms, we

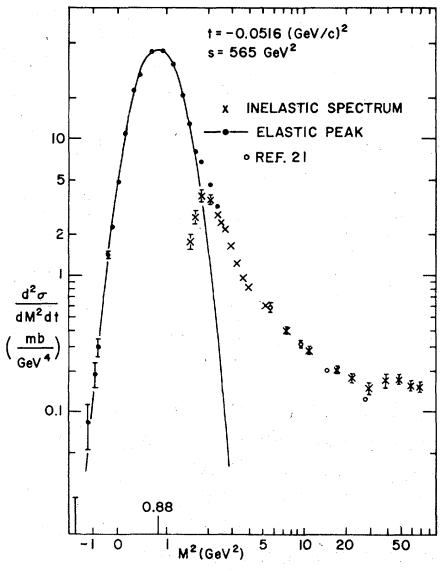

FIG. 6. A typical plot of $d^2\sigma/dtdM^2$ showing our good mass resolution and large mass range. Open circles are from Ref. 21, scaled from $s = 516$ to 566 GeV^2 using our s dependence.

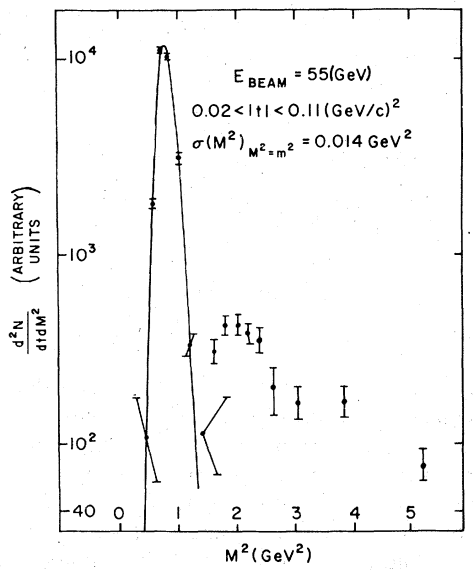

FIG. 7. A plot of the differential cross section showing the unambiguous separation of elastic and inelastic data at low energy.

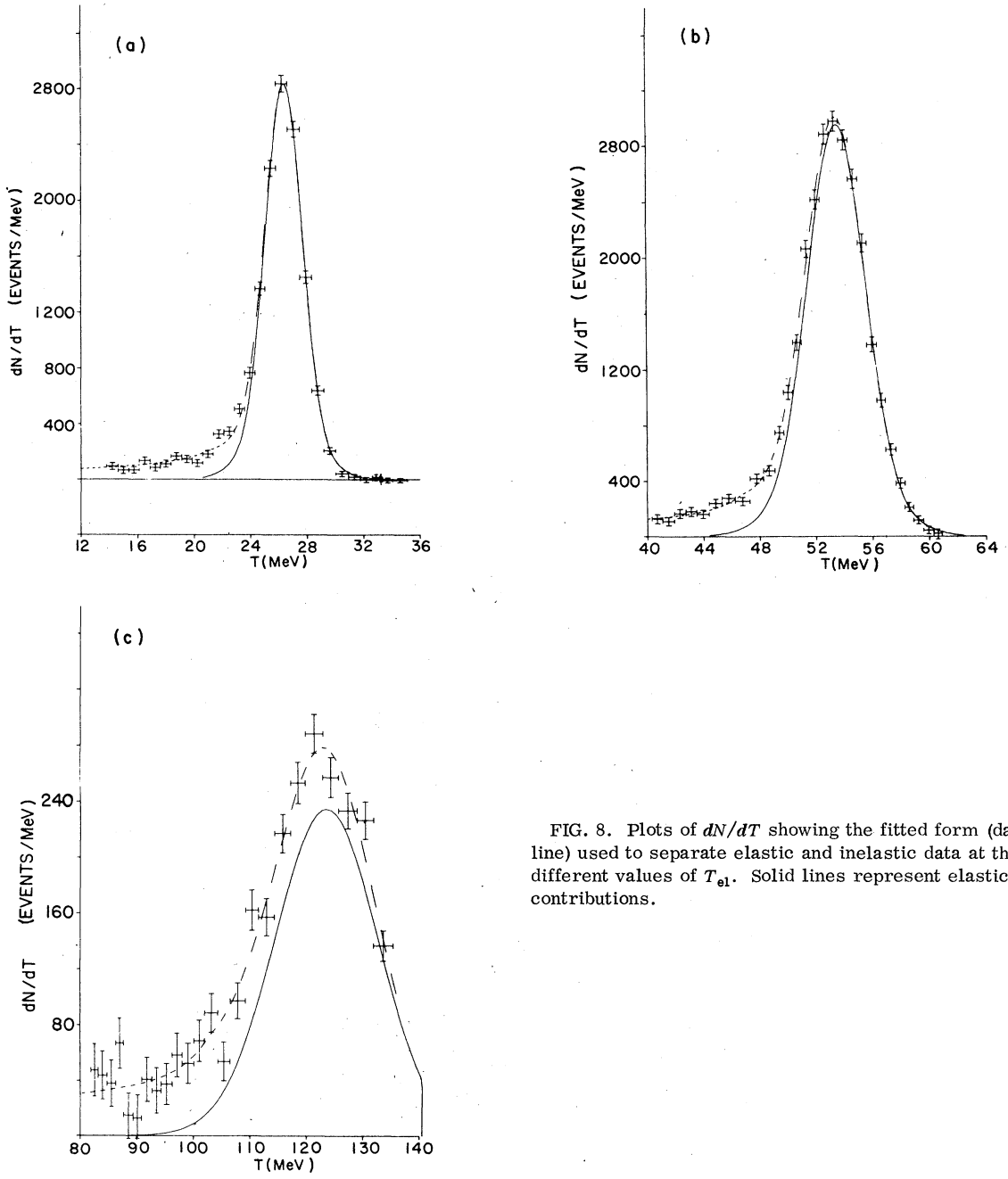

FIG. 8. Plots of dN/dT showing the fitted form (dashed line) used to separate elastic and inelastic data at three different values of T_{el}. Solid lines represent elastic contributions.

prefer to do the separation directly from the $d^2N(s)/dTd\Omega$ mappings because our resolution function in T is independent of beam energy and angle and its parameters can be calibrated at beam energies where the elastic events are separated from the inelastic continuum (from $E_{beam} = 8$ to about 100 GeV). From the knowledge of the T resolution function, the central value of the elastic peak (as measured at low beam energies) and the fact that kinematically the inelastic events must have less energy than elastic events at the same angle, the elastic and inelastic contributions to each measured spectrum are unambigously separated. This separation is very good over our whole T range because of our good resolution (see Sec. II C) and the absence of background. Typical results of such separation are shown in Figs. 8(a), 8(b), and 8(c) up to the highest T. The dashed lines are the fitted curves to the data. The form used to fit was the sum of a δ function at the elastic position and an

arbitrary polynomial which is constrained to vanish above the kinematically allowed maximum T value, folded with our experimentally determined resolution function.

We note that the functional form also includes the multiple-scattering effects from our thin targets which are negligible except at extremely low T (≈15 MeV). The net effect of multiple scattering at $T \approx 15$ MeV is an approximately 100-keV shift of the center and a 1% asymmetric broadening of the peak, almost invisible in Fig. 8(a). At the high end of the T range ($T \sim 100$ MeV), where the elastic contribution has fallen greatly and has become comparable to the inelastic contribution, there is an apparent 1% shift in the elastic peak position due to the two contributions [see Fig. 8(c)]. The aforementioned knowledge of the peak positions at low beam energies, where the inelastic is completely separated from the elastic, allows us to uniquely separate the elastic from inelastic data. Hence throughout our s and T range, we have a complete determination of the relative elastic and inelastic contributions in the dN/dT plot in the elastic region and the elastic contributions (solid lines in said figures) were removed to yield the inelastic contribution. Incidentally, varying the parameters of the resolution function, including width, by a factor of 2 or so, does not affect the inelastic spectrum above mass squared of 2 GeV^2 because our mass resolution is so narrow that only the tail of the inelastic overlaps the elastic region.

C. T dependence of solid-angle acceptance

In any spectrometer, the momentum scale, as well as the system's acceptance as a function of momentum, is obtained by calibration through the incidence of monoenergetic beams upon the system. In our case, the elastic proton recoils provide us

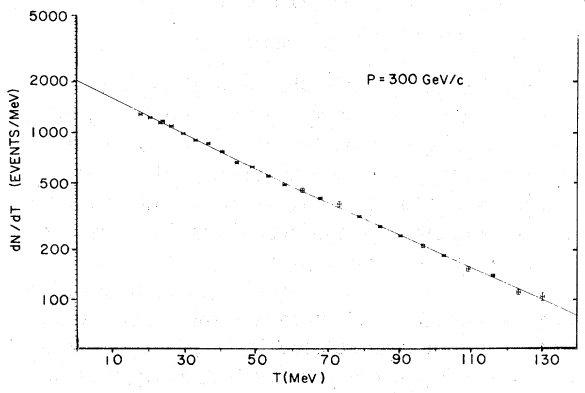

FIG. 9. A plot of dN_{el}/dT for a small set of data at $p = 300$ GeV/c with a fit over two t intervals to the form Ae^{bt}.

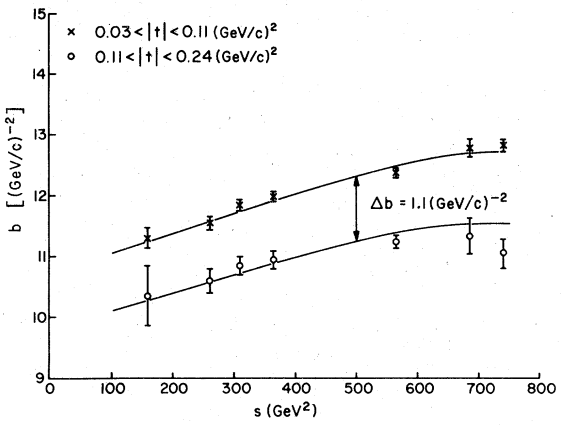

FIG. 10. $b(s)$ vs s for two t intervals. The t dependence of the solid angle has been calibrated using the data of Ref. 16.

with monoenergetic beams throughout our T range. As has been stated in Sec. II C, they allow us to check our $T(E_2)$ function, calibrate the relative $T(E_2)$ functions of each telescope, and the relative acceptances of the telescopes as a function of T, which were identical to within 2%. Finally, they allow us to calibrate our acceptance as a function of T if dN/dT vs T is known at any s. Our acceptance is 95% uniform across our T range. The small nonuniformity exists because detector D_0 has a small effective increase in area for low T (≈15–25 MeV) events. The size of the effect was measured in the following manner: Plots of $d\sigma_{el}/dt$ vs t were first obtained without assuming any T dependence in the solid-angle acceptance (for a typical plot, see Fig. 9, elastics from a subset of data at 300 GeV/c). The t range was split into two pieces, namely, from $0.032 < |t| < 0.113$ and from $0.113 < |t| < 0.234$ (GeV/c)^2. The elastic data were then fit to the form Ae^{bt} over each range but requiring that they have the same value at $t = -0.113$ (GeV/c)^2 ($T = 60$ MeV, close to where we performed the absolute normalization). The slopes so obtained agreed within 10% with those obtained by experiments designed to measure elastic scattering to high precision.[16] Our slope values tended to be high by 1.5 GeV^{-2} in the low-t region and were consistent in the high-t region. This was seen, independent of telescope, runs, and beam energy, confirming its systematic nature in favoring trigger acceptance of low-T events. Therefore, assuming at 200 GeV the correctness of the Fermilab measurement,[16] we have measured our acceptance as a function of T, which can then be applied to all our data at different s values since as stated our resolution function in T and fixed θ is independent of beam energy. Moreover, when such is done, we note that the change in slope between the

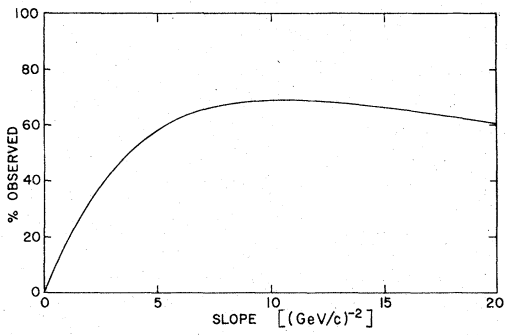

FIG. 11. Fraction of $d\sigma/dt$ measured in the present experiment vs slope parameter for a simple t dependence of the form $\exp(bt)$.

two regions $\Delta b = b_{low\,t} - b_{high\,t}$ is about 1.1 GeV^{-2} and is present over the whole range of our s measurement (see Fig. 10). The magnitude of this effect is in agreement with other measurements at Fermilab and ISR[17] performed at different s values from our experiment. The present data are not accurate enough to differentiate between a "break" and a continuous change in slope of the elastic.

It is noteworthy that one need not even correct this small (5%) lack of uniformity in acceptance over our T range, when considering $d\sigma/dM^2$ (integrated over T) since our range covers 70% of the cross section and the fraction of coverage is identical as long as the slope lies between 6 and 19 (GeV/c)$^{-2}$ (see Fig. 11).

D. Conversion to absolute units

Since the actual beam intensity on target in this experiment was not measured, the cross sections $d^2N(s)/dtdM^2$ were obtained in arbitrary units. The elastic contributions were used to get the normalization constant which transforms from $d^2N/dtdM^2$ to $d^2\sigma/dtdM^2$ for each set of data, in particular we used our measured elastic cross section at $t = -0.094$ (GeV/c)^2 equating it to $d\sigma_{el}/dt$ at the same t [26.65 mb/(GeV/c)^2]. The absolute normalization was performed at this particular t because over our s range of.160 to 741 GeV^2, $d\sigma_{el}/dt$ at $t = -0.094$ (GeV/c)^2 was independent of s to 1% (see Appendix A).

E. Corrections

The corrections necessary in this experiment to be applied to the raw subtracted H_2 spectra are minor (≈2%). Were they not applied at all, the characteristic of the spectra would not have been altered.

There was an unplanned complication at very low T, i.e., 2% of our T range ($T \lesssim 15$ MeV) in the otherwise ideal bin-by-bin $(CH_2)_n - C$ subtraction method used to obtain the free-proton distributions, namely, that the two targets were of different thicknesses, especially since the polypropelene fibers tended to melt in the beam and increase their girth. We recall that our T scale which assigned T values to each bin was determined by the measurement of the elastic proton scattering (knowing the scattering angle), hence correctly represented the energy of the recoil proton from an interaction within the polypropelene fiber, independent of energy loss in escaping the polypropelene target. Therefore a correction factor (1% at 15 MeV, negligible thereafter) dependent on the difference in thickness between the two targets was applied both bin by bin to the carbon proton distrubution and to the deuteron normalization factor before the subtraction was performed. The average thickness of the polypropelene target, weighted by our live time, was calculated using data taken at angles and T values which were kinematically forbidden to free protons (negative mass-squared region), but not to carbon protons with their Fermi momentum, together with the deuteron counts and knowledge of proton to deuteron cross sections as a function of T measured from our previous experiment.[11,15] The target thickness information was thus used in the calculations of the 100-keV shift and 1% asymmetric broadening of elastic peaks due to multiple scattering at low T ($T \approx 15$ MeV) (see Sec. III B). The subsequent modification in T scale and in decrease of events in the polypropelene distribution at low T due to this effect was small (<2%) and was corrected for.

Nuclear interactions in the detectors (which could cause mismeasurement of the total energy) were negligible, giving effects of <1%, and were not corrected for.

IV. RESULTS

A. General features

This experiment resulted in a 4000-point three-dimensional mapping of the doubly differential inelastic cross section $d^2\sigma/dtdM^2$ as a function of s. Innumerous two-dimensional projections were examined during the analysis to decide the best method for synthesizing and extracting physics results from the data. For example, Fig. 12 shows $d^2\sigma/dtdM^2$ for $t = -0.075$ (GeV/c)^2 vs M^2 at three different s values in the low-mass region. The dominant feature clearly is a large peak at low M^2, independent of s, falling sharply as M^2 increases (much sharper than $1/M^2$). The area of this peak is largely independent of s, the height variations seen in the figure just reflect our

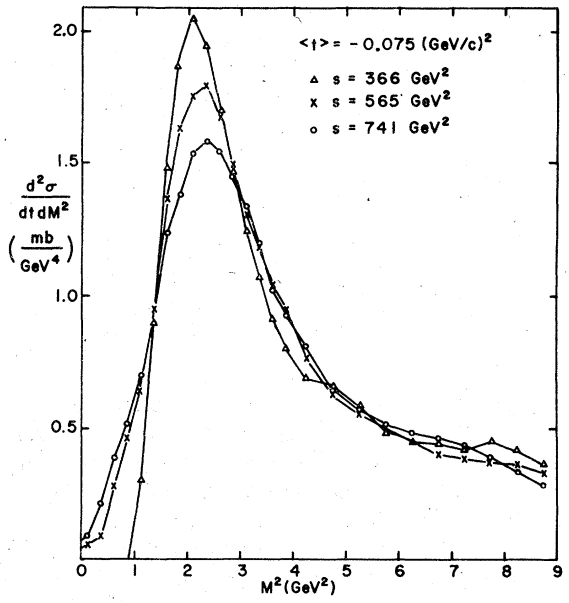

FIG. 12. A plot of the low-mass peak showing that it is essentially independent of s for fixed M^2 (i.e., not for fixed $x = 1 - M^2/s$).

broadening mass resolution with increasing s. Note that the use of the Feynman variable x ($\sim 1 - M^2/s$) as the independent variable in this region would have introduced an apparent energy dependence to this energy-independent peak.

Figure 13 shows $d^2\sigma/dtdM^2$ integrated over our t range (for statistics) for three values of s, emphasizing the high-mass region. The cross sections at large M^2 have leveled out. Also, the three sets of data are vertically displaced by a constant amount for all M^2 values. The value at which the

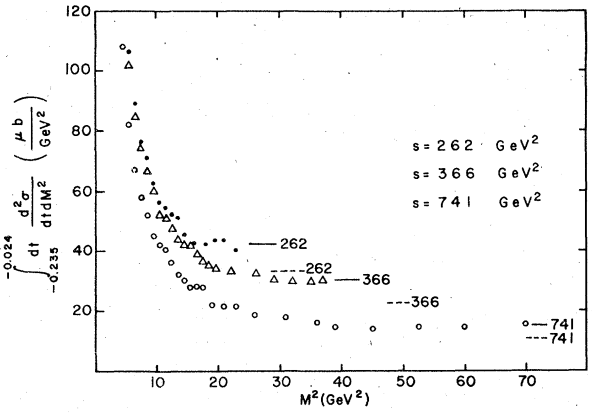

FIG. 13. A plot of the high-mass region showing that the cross section is tending to a constant level whose height appears to vary like $1/s$. The solid lines are the values of $11/s$ at the indicated s. The dashed lines are obtained using the fit of Ref. 19.

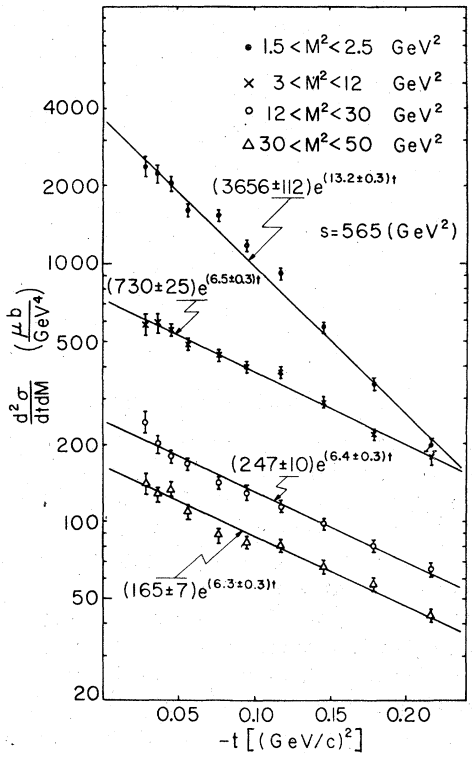

FIG. 14. A plot of t dependence for 4 intervals in M^2 showing that the slope is always > 6 GeV^{-2} justifying our t extrapolation independent of M^2. Note the much steeper slope in the $N(1400)$ region.

cross section appears to level out falls as $1/s$. In fact, the heights marked on the graph with a solid line next to the large-M^2 cross sections are values of $11/s$, evaluated at each appropriate s. These constant separations, moreover, extend down to very low masses, within statistics probably down to threshold (in this figure over the whole mass range plotted).

Figure 14 shows typical t dependence observed in our data at $s = 565$ GeV^2. To reduce statistical fluctuations, the data have been averaged over four large mass intervals. Noteworthy features of our inelastic data t dependence are that for all M^2 regions, values not in the vicinity of $M^2 \approx 2$ GeV^2, i.e., the $N(1470)$, the slopes resulting from fits to the form Ae^{bt} are between 6 and 7 (GeV/c)$^{-2}$ (see Table I). Limited statistics in this experiment do not allow a detailed study of M^2 vs t and s, for example, whether the logarithmic slope b is itself a function of t. Of importance, however, is the fact that this experiment observes about 65% of the total inelastic cross section (per given s and M^2) independent of b as long as the inelastic cross section can reasonably be described by a simple exponential t dependence whose slope lies between 6 and 19 (GeV/c)$^{-2}$ (see Fig. 11).

TABLE I. Slope parameters $b(s)$ in $(\mathrm{GeV}/c)^{-2}$ for inelastic $d^2\sigma/dtdM^2$ at $s = 262, 309, 366, 565, 741$ GeV^2.

M^2 (GeV^2) \ s (GeV^2)	262	309	366	565	741
1.2–2.5	13.7 ± 0.6	14.8 ± 0.6	15.0 ± 0.6	13.2 ± 0.3	13.0 ± 0.5
3–12	6.8 ± 0.6	6.1 ± 0.6	6.2 ± 0.6	6.5 ± 0.3	7.0 ± 0.8
12–20	6.9 ± 0.6	6.9 ± 0.6	7.0 ± 0.6	6.4 ± 0.3	6.4 ± 0.6
30–40			6.0 ± 0.6		
30–50				6.3 ± 0.3	5.9 ± 0.6
50–70					6.5 ± 0.6

B. Integrated cross sections

Aided by the insights obtained from the examination of the aforementioned two-dimensional projections of the data, we decided that cross sections integrated over our range in t and from threshold to various fractions of s: (a) gave a direct measurement of whether the "diffractive" region was responsible for the increase in the total cross section as a function of s, (b) greatly reduced (by a factor of ~100) the number of data points, (c) eliminated the need for detailed knowledge of mass resolution and t dependence as a function of M^2 and still allowed the determination of the mass spectrum as a function of s.

The data presented in Table II were obtained by first summing $d^2\sigma/dtdM^2$ for fixed mass over ten t intervals, from $t = -0.024$ to $t = -0.234$ $(\mathrm{GeV}/c)^2$ and then summing over mass from threshold to $\eta s + m^2$ for five different values of η. These are directly measured quantities which demonstrate that as long as the low-mass peak is included in the cross section measurement, the total cross section in the "diffractive region", i.e., from threshold to any fraction $(0.05 \leq \eta \leq 0.1)$ of s, is essentially independent of s. These cross sections are consistent with an increase with s of the same fractional amount as the total cross section (~5%), and clearly are in contradiction with the postulate that the total rise in cross section of 0.7 to 0.9 mb occurs in this low-mass region. For comparison with other measurements, we extrapolated our measurements to include the remaining t domain by multiplying our results by 1/0.65. The results are plotted in Fig. 15(a) for five different values of η and seven values of s.

The cross section obtained by integrating the data over t and extended using (1/0.65) now has the following uncertainty because of the possibility of a flattening of the inelastic slope at high t[18]: namely, this introduces an asymmetric error (since it is probably not steeper at large t) of $+10\%, -2\%$. This is essentially a scale factor since it is independent of s and M^2.

C. Mass dependence

As we have explained previously, we have a several-thousand-point mapping in $d^2\sigma(s)/dtdM^2$

TABLE II. Integrated cross section vs s:

$$\sigma = \int_{-0.234}^{-0.024} dt \int_{\mathrm{th}}^{\eta s + m^2} dM^2 \left(\frac{d^2\sigma}{dtdM^2}\right),$$

σ in mb, t in $(\mathrm{GeV}/c)^2$, M^2 in GeV^2.

Fraction η \ s (GeV^2)	262	309	366	565	741
0.10	2.00 ± 0.028	2.06 ± 0.028	2.03 ± 0.028	2.02 ± 0.028	2.16 ± 0.030
0.06	1.57 ± 0.026	1.60 ± 0.026	1.59 ± 0.026	1.65 ± 0.026	1.72 ± 0.027
0.04	1.31 ± 0.024	1.33 ± 0.024	1.33 ± 0.024	1.42 ± 0.024	1.49 ± 0.024
0.02	0.93 ± 0.022	0.95 ± 0.022	0.96 ± 0.022	1.11 ± 0.022	1.18 ± 0.022
0.01	0.60 ± 0.020	0.62 ± 0.020	0.64 ± 0.020	0.82 ± 0.020	0.90 ± 0.020

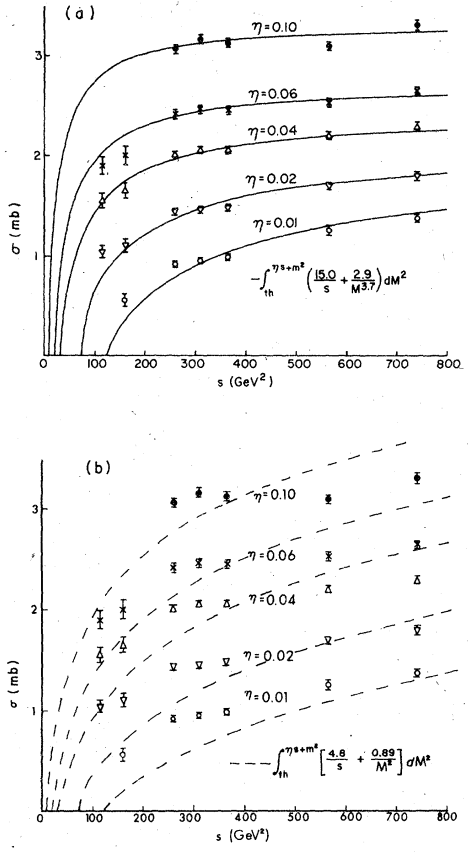

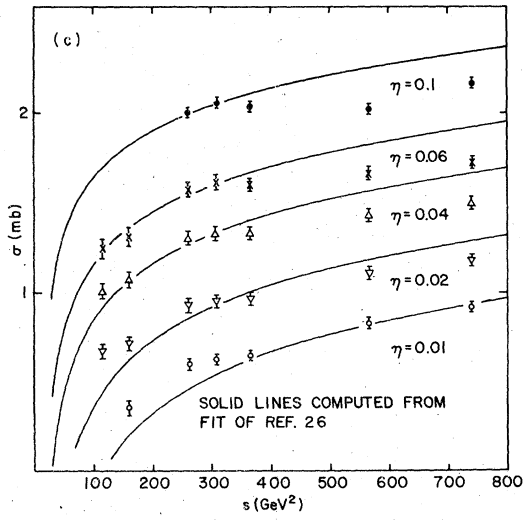

FIG. 15. Integrated cross section vs s. The solid lines in (a) are the best fits to our data as explained in the text. The dashed lines in (b) are the best fits requiring $\alpha = 2$, showing a clear inconsistency. The lines in (c) are computed from the fit of Ref. 26. Note that the data in (c) are the cross sections measured over our t acceptance; in (a) and (b) the cross sections have been extrapolated to the full t range by using the factor 1/0.65, see text.

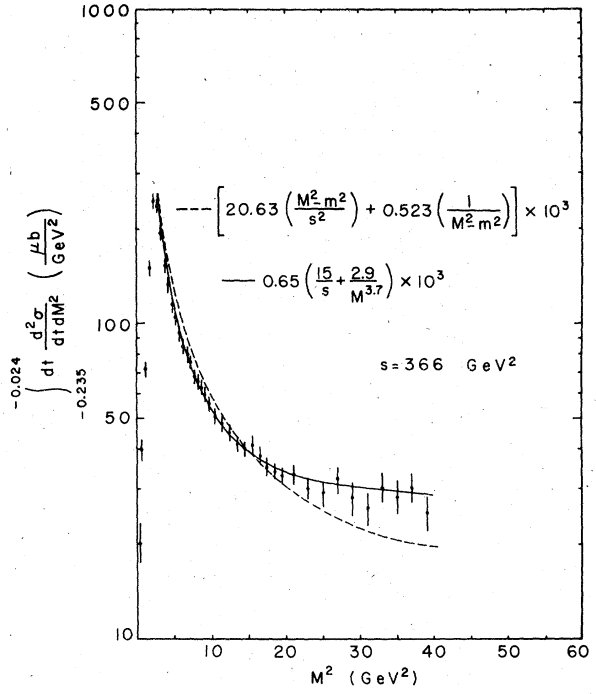

FIG. 16. Mass-squared spectrum at $s = 366$ GeV^2. Solid line is computed from our fit to all our data. Dashed line is computed from a fit to all our data using the parametrization of Ref. 26.

(see Tables III–VII). We felt that it was neither an efficient use of computer time, nor instructive to make a simultaneous fit to this huge three-dimensional array. Furthermore, the low-mass enhancement is full of structures (1400, 1520, 1688, 2190, ..., etc.)[27] and any fit which does not incorporate explicit resonance structure is bound to be poor. The physics question we are asking is, in the spirit of duality, what is the average behavior of the mass spectra? The best way to group data into larger bins, obtaining the correct weighted average, is by integrating the measured distribution over t and various portions of the M^2 spectrum, for example to fixed fractions of s. No information is lost in such a way as long as s and the fractions span enough values to cut deeply into the low-mass enhancement. Thus we fit over a much smaller, more precise and correctly locally smoothed set of data. Once the best fit is found, the resultant fit can be compared with both the measured differential cross sections and with fits obtained from directly fitting individual differential cross sections. We usually do both and obtain excellent agreement between them; of course, the global fit is much more precise. All fits presented in the following were performed using integrated cross sections. The integrated-

cross-section points on Fig. 15 were used to perform a fit to the form $d\sigma/dM^2 = A/s + B/M^\alpha$ suggested by the data itself, yielding $A = 15.0 \pm 0.5$ mb, $B = 2.9 \pm 0.1$ mb GeV$^{1.7}$, and $\alpha = 3.7 \pm 0.1$ with a $\chi^2 = 33$ for 22 degrees of freedom. The low-energy ($s = 114$, 160 GeV^2) points were not used in the fit. However, looking at the points and at the solid lines in Fig. 15(a), which are the above-mentioned fit, one notes that our fitted form is valid down to $s \sim 100$ GeV^2. The solid line in Fig. 16 shows the fitted curve $d\sigma/dM^2 = 15/s + 2.9/M^{3.7}$ superimposed on a typical set of data at $s = 366$ GeV^2, note the excellent agreement.

The degree to which our data rejects other values of α can be seen by the resulting increase in χ^2 values when we impose specific values of α during the fit: $\alpha = 4$, $\chi^2 = 42$; $\alpha = 3$, $\chi^2 = 105$; $\alpha = 2$, $\chi^2 = 1017$. Hence it can be summarized that our data's best fit is $\alpha = 3.7 \pm 0.1$, it could probably accept $\alpha = 4$, it is inconsistent with $\alpha = 3$. It categorically rejects $\alpha = 2$ [see Fig. 15(b)] which is the mass-spectrum dependence which would trivially have predicted that the low-mass region was responsible for the rise in the total cross section with s

$$\left[\int_{\text{th}}^{ns}\left(\frac{A}{M^2}\right)dM^2 = A \times (\ln s + \text{constant})\right].$$

We have tried fitting with other functional forms, all of which give poorer χ^2 values, typically greater than 50. This is because any appreciable mixing of the s and M^2 dependences is at variance with our data. As an example, we have performed a fit to the parametrization presented by Ref. 26:

$$s\frac{d^2\sigma}{dtdM^2} = A_1 \exp(B_1 t + C_1 t^2)[1 + D_1(E_{\text{beam}}^{-1/2} - 0.1)](1-x) + A_2 \exp(B_2 t + C_2 t^2)[1 + D_2(E_{\text{beam}}^{-1/2} - 0.1)]/(1-x),$$

where we have used the values $B_1 = 8.32$ GeV^{-2}, $C_1 = 5.24$ GeV^{-4}, $B_2 = 7.24$ GeV^{-2}, and $C_2 = 2.58$ GeV^{-4} given by Ref. 26 (since they are consistent with our t dependence), obtaining a χ^2 of 54. The dashed curve in Fig. 16 is our fit for this parametrization at $s = 366$ GeV^2. The large value for χ^2 comes from the fact that our mass spectrum is not $1/M^2$ regardless of its s dependence.

D. Magnitude of "diffractive" cross section

According to Good and Walker,[1] inelastic diffraction is independent of s whenever the coherence condition is satisfied; i.e., the change in de Broglie wavelength corresponding to $m \to M$ is smaller than the scatterer's thickness, in our case the proton radius $\approx 1/m_\pi$. From the kinematics this is satisfied for states of mass M such that $M^2 \lesssim s(m_\pi/m) \approx 0.14s$. Hence it is of interest to study the magnitude of such an s independent term in the mass spectrum, as it could be a dominant process at high s where large M^2 values can be coherently produced (50–100 GeV^2 in the present experiment). We identify the B/M^α term of our fit (which is s independent) as the "diffractive" cross section in the Good and Walker sense. Hence the total "diffractive" cross section, taking into account the symmetry of the initial pp state, is $2 \times \int_{\text{th}}^{\infty}(2.9/M^{3.7}) = 3.6 \pm 0.4$ mb. This magnitude is small compared to the total inelastic cross section and is about half of the elastic cross section. Also, the contribution of this diffractive term essentially vanishes at $M^2 \sim 20$ GeV^2, significantly before the maximum mass values allowed by the coherence condition.

E. Comparison with other experiments

The major experimental effort to study pp inelastic scattering at small momentum transfer at ISR was made by the Cern-Holland-Lancaster-Manchester (CHLM) group.[18] There is some overlap in the s, t, and mass regions studied by CHLM ($M^2 < 50$ GeV^2, $0.15 < |t| < 1.75$ (GeV/c)^2, at $s = 549$ GeV^2 and 725 GeV^2) and by this experiment. A few years ago, the Rutgers–Imperial College (RI)

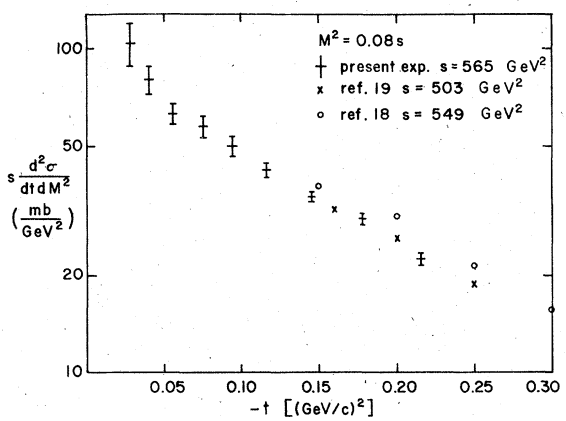

FIG. 17. A comparison of our large-mass data to other experiments, showing good agreement in both slope and magnitude of the inelastic cross section.

collaboration performed an experiment[19] in our s range at Fermilab for a small fraction of the cross section, $0.14<|t|<0.38$ (GeV/c)^2 and $0.07s<M^2<0.2s$. The Fermilab Single Arm Spectrometer Group (FSASG) has published some results[20] for $pp \to pX$ at $s = 296$ GeV^2, $3<M^2<9$ GeV^2, and $0.1<|t|<0.625$ (GeV/c)^2 and more recently a parametrization[26] of $d^2\sigma/dtdM^2$ based on the remainder of their data. In the low-mass, low-t region, we overlap with two Soviet–U.S. efforts,[21] for $0.01<|t|<0.05$ (GeV/c)^2, $1.3<M^2<3.7$ GeV^2, $330<s<752$ GeV^2 from $p+p \to p+X$ and for $0.03<|t|<0.12$ (GeV/c)^2, $M^2<35$ GeV^2 from $p+d \to d+x$ and extracting the nucleon-nucleon cross sections by factorization. Many bubble-chamber experiments studied the reaction $p+p \to p+X$ and collectively they cover a vast s, t, and M^2 range, but are limited by statistics.[22] Finally, there was our previous experiment[11,15] at $s = 569$ GeV^2, covering a similar t range, with M^2 extending to $0.17s$, and there is our current experiment[23] at the ITA using a hydrogen-jet target, where the t range is extended to 0.5 (GeV/c)^2 and the s range is extended to $s = 939$ GeV^2. The present experiment[25] is in agreement with both our previous experiment and with the preliminary results of our current experiment.[27]

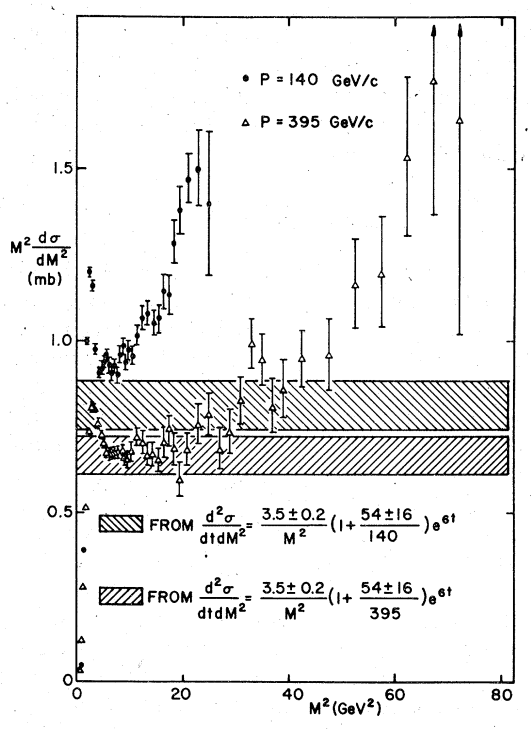

FIG. 18. A plot of $M^2 d\sigma/dM^2$ vs M^2 again showing that our data are inconsistent with a dominant $1/M^2$ mass dependence. Dashed area is prediction of formula of Ref. 21 including errors.

For comparison with other experiments, we note that wherever data overlap and resolution effects have not distorted mass spectra, we and the other experiments agree to within 20%. For example, all the experiments find the inelastic slope b (of Ae^{bt}) to be ~6 (GeV/c)$^{-2}$ for $5<M^2<50$ GeV^2, while around $M^2 \approx 2$ GeV^2 the slope is much larger. In Fig. 17 we see the ISR[18] and RI[19] points superimposed over ours, showing agreement in both magnitude and t dependence of the differential cross section at large mass and high t. In Fig. 12, the value of $d\sigma/dM^2$ (the dashed lines) calculated from the RI formula is shown next to our data. These lines indicate that the s dependence of their prediction agrees with our data but their formula underestimates the cross section in our region. In Fig. 6, four points from the Soviet–U.S. collaboration are plotted (adjusting for the fact that their measurements were made at $s = 516$ instead of 565 GeV^2 by using our s dependence), again exhibiting that there is no significant divergence of experimental values. Inspection (see Appendix B) of our cross section values in the s, t, and M^2 ranges which overlap those of FSASG clearly indicate agreement. This is also shown by the respective values of the parameters A_1 and A_2. We obtain $A_1 = 484 \pm 116$, $A_2 = 6.6 \pm 0.1$ while FSASG reports[26], $A_1 = 612 \pm 30$, $A_2 = 6.1 \pm 0.4$. Finally, we note that ISR finds $2\times\int_{\text{th}}^{0.1}(d\sigma/dM^2)dM^2$ to be 7.61 ± 0.23 mb at $s = 549$ GeV^2 and to be 7.24 ± 0.53 mb at $s = 725$ GeV^2, having extrapolated to include the unmeasured $|t| < 0.15$ (GeV/c)^2 region. From Fig. 15(a), one sees that our corresponding two values are 6.44 ± 0.38 mb at $s = 549$ GeV^2 and 6.53 ± 0.34 mb at $s = 725$ GeV^2.

We recall that these integrals were obtained by extrapolating over the remaining t domain unmeasured by us by assuming a simple exponential. However, if the inelastic slope indeed flattens out at high t as measured at ISR [b goes from 6 to 4 (GeV/c)$^{-2}$)] then our values should be revised upwards by ~10%. Hence the comparison is between 7.61 and 7.08 mb at $s = 549$ GeV^2, and between 7.24 and 7.15 mb at $s = 725$ GeV^2, clearly in good agreement.

The CHLM experiment, however, reports a spectrum like $1/M^2$. Since we have shown that both our integrated- and high-mass cross sections agree well with their results, we suggest that the different shape observed at ISR is due to the wider M^2 resolution (~10 GeV^2) of their experiment. An indication of the distortion of the mass spectrum due to poor mass resolution can be obtained by folding their quoted resolution into our data.[23] This produces a decrease in the cross section at $M^2 = 0.005s$ of a factor of two. The FSASG and the

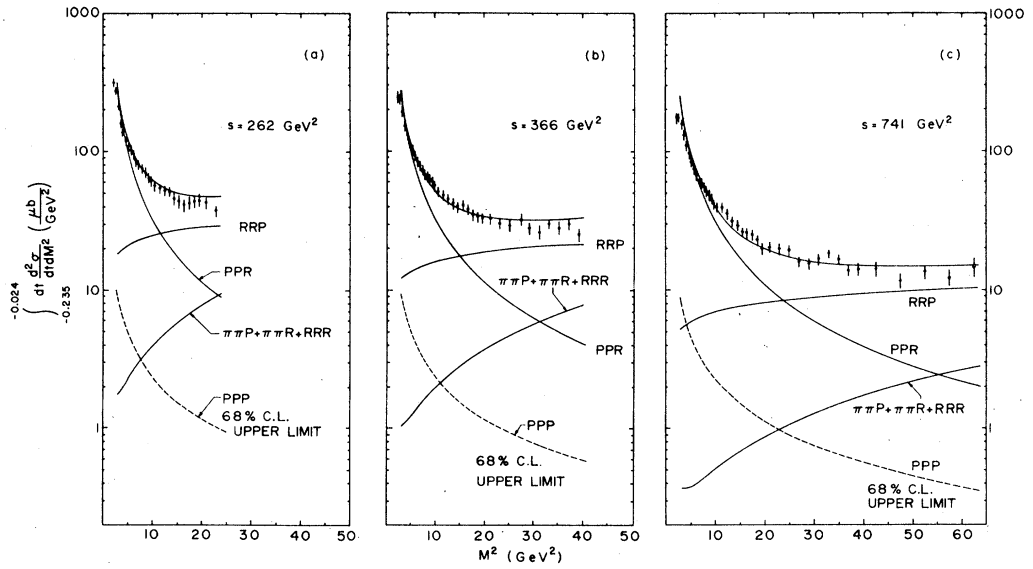

FIG. 19. Comparison of triple-Regge analysis of all our data with spectra measured at three s values. Also indicated are the contributions of various terms. The result of the fit for the PPP term, constrained to be positive, is 0 and the upper limit (68% confidence level) is shown.

Soviet–U.S. collaborations also quote a $1/M^2$ mass spectrum, modified by a partial s dependence. In these cases we believe that it is the limited range of their M^2 measurement which led to such a formulation. This is best demonstrated in Fig. 18 where $M^2 d\sigma/dM^2$ is shown for two s values together with the Soviet–U.S. formula prediction. It is apparent that $M^2 d\sigma/dM^2$ is flat for only a very narrow region of M^2 and that region is different for different s values, hence $1/M^2$ cannot be the correct mass-spectrum dependence for the s independent part of the cross section. Figure 15(c) shows the FSASG[26] formula superimposed on our data. Agreement is good in the overlapping s region but apparently the formula is not valid at higher s values.

F. Comparison with theoretical conjectures

While our fitted spectrum is of the form $d\sigma/dM^2 = 15/s + 2.9/M^{3.7}$, dimensional arguments suggest for the energy-independent cross section $d\sigma/dM^2 = \text{constant}/M^4$. Similarly, for the scaling term, the only scale is fixed by σ_{tot}, resulting in $d\sigma/dM^2 = g(M^2/s) \times (\sigma_{\text{tot}}/s)$, where $g(M^2/s)$ appears to be remarkably constant up to $M^2/s \sim 0.1$. It is therefore logical that the inelastic spectrum should be of the form $d\sigma/dM^2 = A/s + B/M^4$. If we constrain $\alpha = 4$, we obtain $A = 16.0 \pm 0.5$ mb and $B = 3.5 \pm 0.1$ mb GeV^2, with $\chi^2 = 42$ for 23 degrees of freedom.

We believe that we have separated the energy-independent part of the cross section from the rest of the inelastic cross section. Its value is 3.6 $\pm$ 0.4 mb and we believe it is the cross section due to coherent dissociation of the beam proton across the depth of the target proton, i.e., σ_{diff}. We note that this value does not contradict the Pumplin bound $\sigma_{\text{diff}} < \frac{1}{2}\sigma_{\text{tot}} - \sigma_{\text{el}} \simeq 13$ mb, or the ratio $R(s) = (\sigma_{\text{el}} + \sigma_{\text{diff}})/\sigma_{\text{tot}}$, determined by us to be ~0.25, half of the saturation value of 0.5.

For completeness, we have also fit our results to the triple-Regge[10] formula for the inclusive inelastic cross section:

$$s\frac{d^2\sigma}{dtdM^2} = \frac{1}{s}\sum_{ijk} G_{ijk}(t)\left(\frac{s}{\nu}\right)^{\alpha_i(t)+\alpha_j(t)}\nu^{\alpha_k(0)},$$

where ijk are PPP, PRP, RRP, PPR, PRR, RRR, $\pi\pi P$, and $\pi\pi R$; P is the Pomeron; R is the Reggeon; $\nu = M^2 - m^2 - t$; $\alpha_P(t) = 1 + 0.28t$ (obtained from Ref. 24); $\alpha_R(t) = 0.5 + t$; $\alpha_\pi(t) = 0 + t$. Following the example of Field and Fox, we ignored the contribution of the interference terms (PRP, PRR) and constrained the $\pi\pi P$, $\pi\pi R$, and RRR contributions to the preferred values used in Ref. 10 (i.e., solution 1). Incidentally the contribution of these three terms agree with our fitted value for the parameter A_2 of Ref. 26 (the $\pi\pi P$ type contribution).

If the G_{ijk}'s are not constrained to be positive, we obtain a negative contribution to the cross section from the triple-Pomeron (PPP) term. Since this is unphysical, we have constrained the G_{ijk}'s to be positive for the fit, giving a χ^2 of 54. Figure 19 shows a comparison of the triple-Regge analysis with mass spectra measured at three s values. Also indicated are the contributions of the various

terms. Since the fit gives the triple-Pomeron contribution to be zero, we have plotted the (68% confidence level) upper limit for this contribution. A comparison of our fit to the preferred solution of Field and Fox (solution 1) gives very different contributions to the cross section from the various terms. For example, integrating Field and Fox solution 1 at $s = 565$ GeV^2 over our t range and for threshold $< M^2 < 0.1\,s$ results in 51% of the cross section being due to the PPP term, 34% comes from the PPR terms, 9% from RRP, and 6% from the combined $RRR + \pi\pi P + \pi\pi R$ terms. However, from our fit to our data, we obtain 0%, 64%, 30%, and 6%, respectively; the strong disagreement is of course another consequence of the fact that our mass spectrum falls faster than $1/M^2$. Moreover, since the fit is poor we conclude that our data are not well described by the triple Regge phenomenolgy.

ACKNOWLEDGMENT

We wish to thank the staff of the Fermilab Accelerator Divison, especially the internal-target-area operating crew and Dr. Drasko Jovanovic; the Nevis machine shop where most of the mechanical construction was performed, and A. Teho for the design work; the Nevis electronics shop and Tom Tarantowitz of Stony Brook for construction of some of the electronics; W. Sippach of Nevis Lab for help with developing the Event Analyzer. This research was supported in part by the National Science Foundation.

APPENDIX A: ABSOLUTE NORMALIZATION

Elastic peaks as a function of T were fit to obtain the number of events per millibarn of elastic cross section. This was the number of events per millibarn used to normalize the inelastic data to obtain the cross section. We have used the value 50.0 mb per GeV for $d\sigma_{el}/dT$ at $T = 50$ MeV for all s. If a small s dependence of $d\sigma_{el}/dT$ at $T = 50$ MeV were observed, our data at any energy could be renormalized by multiplying all the data points by the appropriate s-dependent constant.

The absolute normalization was done at $T = 50$ MeV because $d\sigma_{el}/dT$ at $t = -0.094$ (GeV/c)^2 is relatively independent of s. The following values as a function of s were obtained[24] from $b(s) = 8.23 + 2 \times 0.278 \times \ln(s)$ (GeV/c)$^{-2}$ and $\sigma_{tot}(s) = 38.2 + 0.49 \times \ln^2(s/122)$ mb:

s (GeV^2)	$d\sigma_{el}/dT\|_{T=50\ \mathrm{MeV}}$ (μb/MeV)
114	51.0
160	50.2
262	49.6
309	49.5
366	49.5
565	49.8
741	50.2
Average	50.0

APPENDIX B: DIFFERENTIAL-CROSS-SECTION TABLES

Tables III–VII consist of five sets (one for each average s value) of $d^2\sigma/dtdM^2$. Each table has four bins in t, the average value of which heads each column, and has up to sixty bins in mass squared, the average value of which labels each row. The four t bins are from $13 \leq T \leq 25$ MeV, $25 \leq T \leq 55$ MeV, $55 \leq T$ 85 MeV, and $85 \leq T \leq 125$ MeV, respectively. Each bin consists of two numbers, the value of the cross section and its diagonal error. A zero error means that no determination of the cross section has been made for that bin. The errors are statistical, and they usually dominate over any systematic errors in subtraction or normalization for different angles. The only exception is the data at the lowest t column, near the $N^*(1400)$ peak where the statistical error is small ($\simeq 1\%$) but the error (which is an estimate of the uncertainty in the calculation) due to uncertainty in size and shape of the target thickness is about 10%. For all other t columns, that uncertainty is negligible (<1%). Finally, if the t dependence at low t as measured by the quoted Fermilab experiment[16] were incorrect, our data should then be corrected by some t-dependent "solid-angle" effect, and the correction would be independent of s and M^2.

TABLE III. $d^2\sigma/dtdM^2$ in μb/GeV^4 at $s = 262$ GeV^2.

M^2 (GeV^2) \ T (MeV) / t [(GeV/c)^2]	19 −0.036	40 −0.075	70 −0.131	105 −0.197
−25				0 ± 8
−15			8 ± 12	2 ± 4
−9.5			14 ± 14	8 ± 8
−8.5			−10 ± 15	9 ± 8
−7.5		−40 ± 56	−6 ± 15	4 ± 7
−6.5		−4 ± 32	22 ± 17	−1 ± 9

TABLE III. (*Continued*)

M^2 (GeV^2) \ T (MeV) / t [(GeV/c)^2]	19 −0.036	40 −0.075	70 −0.131	105 −0.197
−5.5		−4 ± 26	1 ± 18	−3 ± 9
−4.5		18 ± 22	7 ± 18	−5 ± 8
−3.5		15 ± 20	−14 ± 16	−2 ± 8
−2.5		−11 ± 18	8 ± 14	19 ± 8
−1.5		8 ± 17	−4 ± 14	23 ± 7
−0.875	24 ± 77	0 ± 20	1 ± 19	39 ± 8
−0.625	25 ± 60	5 ± 19	−4 ± 18	47 ± 9
−0.375	45 ± 56	13 ± 21	14 ± 18	52 ± 10
−0.125	35 ± 54	22 ± 26	17 ± 17	57 ± 11
0.125	95 ± 72	44 ± 32	49 ± 21	70 ± 12
0.375	170 ± 89	65 ± 39	65 ± 29	85 ± 14
0.625	313 ± 107	114 ± 46	107 ± 29	111 ± 17
0.875	506 ± 121	201 ± 54	152 ± 35	189 ± 20
1.125	876 ± 107	381 ± 46	259 ± 31	252 ± 18
1.375	1553 ± 89	738 ± 39	412 ± 28	323 ± 15
1.625	2750 ± 72	1286 ± 32	606 ± 21	383 ± 14
1.875	4109 ± 56	1940 ± 26	814 ± 17	439 ± 12
2.125	4291 ± 54	2172 ± 22	1066 ± 16	496 ± 10
2.375	3661 ± 56	2131 ± 21	1106 ± 17	542 ± 9
2.625	3033 ± 58	1964 ± 21	1101 ± 16	560 ± 7
2.875	2624 ± 61	1759 ± 20	1056 ± 15	547 ± 7
3.125	2054 ± 62	1495 ± 21	957 ± 15	533 ± 7
3.375	1530 ± 63	1225 ± 21	846 ± 15	516 ± 7
3.625	1285 ± 59	984 ± 21	763 ± 16	487 ± 7
3.875	1229 ± 57	865 ± 22	700 ± 18	453 ± 7
4.25	1132 ± 48	765 ± 20	606 ± 18	412 ± 8
4.75	1156 ± 49	703 ± 22	516 ± 19	354 ± 9
5.25	1028 ± 57	675 ± 20	435 ± 19	330 ± 8
5.75	987 ± 58	656 ± 20	376 ± 18	305 ± 8
6.25	994 ± 55	575 ± 20	348 ± 17	264 ± 8
6.75	892 ± 51	502 ± 20	339 ± 16	226 ± 8
7.25	877 ± 48	454 ± 21	342 ± 17	201 ± 8
7.75	736 ± 50	392 ± 22	342 ± 18	196 ± 8
8.25	747 ± 51	408 ± 21	330 ± 18	188 ± 8
8.75	729 ± 49	448 ± 19	285 ± 17	172 ± 8
9.25	542 ± 47	423 ± 19	281 ± 16	160 ± 9
9.75	557 ± 46	389 ± 21	269 ± 15	159 ± 9
10.5	622 ± 38	339 ± 18	222 ± 14	143 ± 8
11.5	613 ± 38	327 ± 18	234 ± 15	121 ± 8
12.5	563 ± 39	340 ± 18	219 ± 17	117 ± 9
13.5	588 ± 39	273 ± 17	206 ± 17	126 ± 9
14.5	491 ± 39	261 ± 18	182 ± 17	127 ± 10
15.5	344 ± 40	296 ± 19	190 ± 16	114 ± 10
16.5	394 ± 44	285 ± 19	203 ± 18	82 ± 9
17.5	461 ± 52	227 ± 19	172 ± 20	83 ± 9
18.5	494 ± 62	263 ± 19	142 ± 17	116 ± 9
19.5	495 ± 68	293 ± 19	122 ± 17	128 ± 10
21	397 ± 64	313 ± 19	146 ± 17	115 ± 10
23	332 ± 79	280 ± 25	154 ± 20	103 ± 16
25	288 ± 107	209 ± 28	170 ± 24	98 ± 14
27		210 ± 31	103 ± 24	93 ± 13
29		124 ± 37	134 ± 27	130 ± 18
31		139 ± 47	106 ± 27	85 ± 25
33		261 ± 57	107 ± 30	118 ± 23
35			85 ± 33	140 ± 21
37			63 ± 42	101 ± 20
39			98 ± 56	45 ± 22
42.5				42 ± 25

TABLE IV. $d^2\sigma/dtdM^2$ in μb/GeV^4 at $s=309$ GeV^2.

M^2 (GeV^2) \ T (MeV) / t [(GeV/c)^2]	19 −0.036	40 −0.075	70 −0.131	105 −0.197
−25				9 ± 4
−15			−7 ± 7	−1 ± 3
−9.5			3 ± 10	5 ± 5
−8.5		24 ± 28	9 ± 10	1 ± 5
−7.5		−4 ± 20	11 ± 11	4 ± 5
−6.5		−4 ± 17	−4 ± 11	14 ± 5
−5.5		6 ± 15	2 ± 11	10 ± 5
−4.5		−4 ± 13	0 ± 10	2 ± 5
−3.5		−5 ± 12	15 ± 9	20 ± 5
−2.5		1 ± 12	4 ± 9	42 ± 5
−1.5	13 ± 53	3 ± 11	27 ± 9	60 ± 6
−0.875	−7 ± 41	18 ± 13	58 ± 11	68 ± 7
−0.625	2 ± 37	19 ± 12	65 ± 10	69 ± 9
−0.375	30 ± 35	15 ± 13	68 ± 10	66 ± 11
−0.125	54 ± 41	48 ± 16	78 ± 12	73 ± 13
0.125	82 ± 49	75 ± 20	54 ± 14	84 ± 16
0.375	118 ± 60	101 ± 23	70 ± 17	108 ± 18
0.625	188 ± 70	136 ± 26	78 ± 19	144 ± 20
0.875	439 ± 81	223 ± 30	126 ± 21	200 ± 21
1.125	726 ± 70	382 ± 27	220 ± 19	246 ± 20
1.375	1342 ± 60	609 ± 23	317 ± 17	285 ± 18
1.625	2274 ± 49	970 ± 20	454 ± 14	341 ± 17
1.875	3693 ± 41	1543 ± 17	621 ± 12	384 ± 13
2.125	4064 ± 35	1949 ± 15	838 ± 10	420 ± 11
2.375	3615 ± 36	1993 ± 13	982 ± 9	441 ± 9
2.625	2909 ± 37	1877 ± 13	1034 ± 10	465 ± 7
2.875	2334 ± 38	1672 ± 13	1018 ± 10	484 ± 6
3.125	1964 ± 39	1433 ± 13	951 ± 9	482 ± 4
3.375	1592 ± 39	1153 ± 13	862 ± 9	477 ± 4
3.625	1317 ± 40	959 ± 13	772 ± 9	466 ± 4
3.875	1167 ± 40	863 ± 14	700 ± 9	447 ± 5
4.25	1068 ± 34	758 ± 13	607 ± 10	413 ± 4
4.75	1069 ± 33	677 ± 13	517 ± 10	373 ± 5
5.25	1027 ± 30	618 ± 14	460 ± 11	333 ± 6
5.75	915 ± 35	549 ± 13	426 ± 11	296 ± 5
6.25	869 ± 42	515 ± 13	390 ± 11	263 ± 5
6.75	824 ± 37	505 ± 12	362 ± 10	233 ± 5
7.25	751 ± 31	467 ± 12	325 ± 10	210 ± 4
7.75	724 ± 30	437 ± 12	315 ± 10	195 ± 5
8.25	719 ± 30	415 ± 13	301 ± 10	190 ± 5
8.75	651 ± 31	353 ± 13	266 ± 10	180 ± 5
9.25	608 ± 32	313 ± 13	241 ± 10	175 ± 5
9.75	580 ± 33	325 ± 13	244 ± 11	167 ± 6
10.5	561 ± 27	324 ± 11	240 ± 9	158 ± 5
11.5	541 ± 26	307 ± 11	227 ± 9	140 ± 6
12.5	524 ± 26	272 ± 11	215 ± 10	115 ± 5
13.5	502 ± 26	270 ± 11	190 ± 10	109 ± 5
14.5	470 ± 26	248 ± 11	188 ± 10	118 ± 5
15.5	430 ± 25	251 ± 11	178 ± 10	119 ± 6
16.5	444 ± 25	248 ± 11	187 ± 10	123 ± 6
17.5	394 ± 25	235 ± 11	189 ± 10	119 ± 6
18.5	366 ± 27	234 ± 11	161 ± 11	101 ± 6
19.5	396 ± 29	227 ± 12	157 ± 11	90 ± 6
21	371 ± 29	200 ± 10	149 ± 9	92 ± 5
23	355 ± 37	206 ± 10	128 ± 10	87 ± 5
25	389 ± 42	223 ± 13	145 ± 10	84 ± 6
27	417 ± 50	201 ± 16	149 ± 11	88 ± 8
29	354 ± 67	201 ± 18	141 ± 13	99 ± 9

TABLE IV. (*Continued*)

M^2 (GeV^2) \ T (MeV) / t [(GeV/c)^2]	19 −0.036	40 −0.075	70 −0.131	105 −0.197
31	415 ± 115	184 ± 19	123 ± 19	87 ± 9
33		194 ± 21	141 ± 20	69 ± 10
35		170 ± 25	125 ± 19	87 ± 10
37		143 ± 30	117 ± 20	87 ± 11
39		112 ± 37	156 ± 23	82 ± 12
42.5		158 ± 57	110 ± 21	71 ± 11
47.5			170 ± 33	60 ± 17

TABLE V. $d^2\sigma/dtdM^2$ in μb/GeV^4 at $s = 366$ GeV^2.

M^2 (GeV^2) \ T (MeV) / t [(GeV/c)^2]	19 −0.036	40 −0.075	70 −0.131	105 −0.197
−35				8 ± 6
−25				3 ± 3
−15		30 ± 32	3 ± 5	2 ± 3
−9.5		−20 ± 20	−1 ± 9	4 ± 4
−8.5		−6 ± 17	3 ± 10	4 ± 4
−7.5		11 ± 14	10 ± 10	0 ± 4
−6.5		15 ± 13	4 ± 10	2 ± 4
−5.5		1 ± 12	−2 ± 9	8 ± 4
−4.5		−1 ± 11	3 ± 8	18 ± 4
−3.5		12 ± 12	15 ± 8	33 ± 4
−2.5		−2 ± 11	12 ± 9	47 ± 4
−1.5	−38 ± 41	6 ± 11	28 ± 8	65 ± 5
−0.875	−14 ± 33	5 ± 12	50 ± 10	72 ± 6
−0.625	14 ± 30	23 ± 12	43 ± 9	77 ± 8
−0.375	36 ± 30	31 ± 11	46 ± 12	77 ± 10
−0.125	84 ± 32	41 ± 14	50 ± 16	89 ± 12
0.125	80 ± 44	73 ± 20	20 ± 70	108 ± 14
0.375	138 ± 54	102 ± 25	120 ± 24	136 ± 16
0.625	258 ± 65	117 ± 30	144 ± 26	161 ± 18
0.875	387 ± 75	230 ± 35	191 ± 31	205 ± 20
1.125	671 ± 66	292 ± 30	240 ± 27	237 ± 18
1.375	997 ± 55	445 ± 25	304 ± 24	278 ± 16
1.625	1823 ± 46	679 ± 20	381 ± 19	315 ± 14
1.875	2921 ± 35	1027 ± 14	522 ± 17	340 ± 12
2.125	3521 ± 31	1544 ± 12	710 ± 12	366 ± 10
2.375	3433 ± 31	1809 ± 12	854 ± 9	381 ± 8
2.625	2932 ± 31	1765 ± 12	937 ± 8	397 ± 6
2.875	2493 ± 32	1611 ± 12	925 ± 8	409 ± 5
3.125	2056 ± 33	1401 ± 12	877 ± 8	411 ± 3
3.375	1636 ± 33	1178 ± 12	814 ± 8	411 ± 4
3.625	1391 ± 33	1007 ± 12	745 ± 8	410 ± 4
3.875	1214 ± 35	869 ± 12	681 ± 8	404 ± 4
4.25	1107 ± 34	762 ± 12	614 ± 8	389 ± 4
4.75	958 ± 33	662 ± 12	520 ± 9	354 ± 4
5.25	851 ± 31	623 ± 12	453 ± 9	322 ± 4
5.75	814 ± 29	548 ± 12	390 ± 9	294 ± 5
6.25	774 ± 28	465 ± 13	367 ± 10	265 ± 5
6.75	733 ± 33	441 ± 13	342 ± 10	243 ± 4
7.25	751 ± 38	429 ± 12	302 ± 9	227 ± 4
7.75	651 ± 35	397 ± 12	276 ± 9	210 ± 4
8.25	572 ± 32	416 ± 12	257 ± 9	199 ± 4

TABLE V. (*Continued*)

M^2 (GeV^2) \ T (MeV) / t [(GeV/c)^2]	19 −0.036	40 −0.075	70 −0.131	105 −0.197
8.75	561 ± 32	388 ± 12	265 ± 8	180 ± 4
9.25	565 ± 31	354 ± 12	262 ± 8	165 ± 4
9.75	549 ± 31	316 ± 13	259 ± 9	154 ± 4
10.5	468 ± 27	291 ± 12	229 ± 9	144 ± 4
11.5	486 ± 25	276 ± 12	200 ± 9	139 ± 5
12.5	443 ± 24	260 ± 12	191 ± 8	133 ± 5
13.5	430 ± 24	233 ± 11	176 ± 8	127 ± 5
14.5	436 ± 23	223 ± 11	167 ± 8	116 ± 5
15.5	474 ± 23	233 ± 11	173 ± 9	101 ± 5
16.5	411 ± 24	221 ± 11	169 ± 9	90 ± 5
17.5	373 ± 23	215 ± 11	153 ± 9	84 ± 5
18.5	343 ± 23	219 ± 12	128 ± 9	89 ± 5
19.5	340 ± 23	203 ± 11	123 ± 9	88 ± 5
21	344 ± 20	208 ± 11	138 ± 8	82 ± 5
23	332 ± 23	183 ± 11	128 ± 8	66 ± 4
25	327 ± 29	174 ± 11	113 ± 8	72 ± 4
27	300 ± 34	203 ± 11	126 ± 9	89 ± 5
29	296 ± 38	167 ± 12	105 ± 10	79 ± 6
31	270 ± 44	142 ± 15	91 ± 12	84 ± 7
33	259 ± 57	185 ± 18	128 ± 15	84 ± 9
35	213 ± 68	184 ± 18	119 ± 16	80 ± 12
37	270 ± 115	168 ± 19	146 ± 17	77 ± 12
39		129 ± 20	122 ± 18	70 ± 9
42.5		113 ± 24	111 ± 13	69 ± 8
47.5			111 ± 17	71 ± 11
52.5				50 ± 11
57.5				19 ± 20

TABLE VI. $d^2\sigma/dtdM^2$ in μb/GeV^4 at $s = 565$ GeV^2.

M^2 (GeV)^2 \ T (MeV) / t [(GeV/c)^2]	19 −0.036	40 −0.075	70 −0.131	105 −0.197
−45				2 ± 1
−35			7 ± 6	1 ± 1
−25			−4 ± 2	1 ± 1
−15		−8 ± 4	−7 ± 1	1 ± 1
−9.5		−1 ± 5	−8 ± 3	3 ± 2
−8.5		−2 ± 5	0 ± 2	4 ± 2
−7.5		−1 ± 5	4 ± 2	4 ± 2
−6.5	−45 ± 148	−4 ± 5	3 ± 2	10 ± 2
−5.5	90 ± 106	−4 ± 5	5 ± 3	15 ± 2
−4.5	−34 ± 35	−3 ± 6	10 ± 3	20 ± 2
−3.5	14 ± 20	−3 ± 6	21 ± 3	25 ± 2
−2.5	13 ± 14	4 ± 5	40 ± 3	41 ± 3
−1.5	9 ± 11	42 ± 5	64 ± 3	71 ± 4
−0.875	18 ± 11	27 ± 5	70 ± 3	92 ± 5
−0.625	48 ± 10	32 ± 5	75 ± 4	108 ± 7
−0.375	52 ± 9	76 ± 6	75 ± 5	122 ± 8
−0.125	89 ± 11	78 ± 8	85 ± 6	143 ± 8
0.125	142 ± 14	137 ± 9	116 ± 7	163 ± 9
0.375	234 ± 17	124 ± 11	166 ± 8	171 ± 10
0.625	359 ± 20	198 ± 12	251 ± 9	188 ± 11

TABLE VI. (*Continued*)

M^2 (GeV)^2 \ T (MeV) / t [(GeV/c)^2]	19 −0.036	40 −0.075	70 −0.131	105 −0.197
0.875	565 ± 22	345 ± 14	333 ± 10	203 ± 13
1.125	889 ± 20	546 ± 12	442 ± 9	220 ± 12
1.375	1323 ± 17	846 ± 11	546 ± 8	237 ± 10
1.625	1893 ± 14	1154 ± 9	628 ± 7	247 ± 9
1.875	2388 ± 11	1435 ± 8	710 ± 6	257 ± 8
2.125	2656 ± 9	1560 ± 6	754 ± 5	270 ± 7
2.375	2715 ± 10	1584 ± 5	774 ± 4	272 ± 6
2.625	2537 ± 10	1493 ± 5	774 ± 3	279 ± 5
2.875	2269 ± 10	1360 ± 5	762 ± 2	277 ± 5
3.125	1895 ± 10	1168 ± 4	738 ± 2	274 ± 4
3.375	1625 ± 10	1049 ± 5	700 ± 3	272 ± 3
3.625	1354 ± 10	914 ± 5	651 ± 3	267 ± 3
3.875	1171 ± 11	825 ± 5	607 ± 3	266 ± 2
4.25	1014 ± 12	730 ± 5	553 ± 3	258 ± 2
4.75	829 ± 12	615 ± 6	467 ± 3	251 ± 2
5.25	753 ± 13	539 ± 6	410 ± 3	239 ± 1
5.75	678 ± 12	489 ± 6	360 ± 3	235 ± 1
6.25	602 ± 12	441 ± 6	321 ± 3	219 ± 1
6.75	559 ± 12	404 ± 6	296 ± 3	205 ± 1
7.25	507 ± 11	368 ± 6	274 ± 3	192 ± 1
7.75	491 ± 12	345 ± 6	255 ± 3	181 ± 1
8.25	460 ± 11	326 ± 6	243 ± 3	169 ± 1
8.75	433 ± 11	307 ± 6	224 ± 3	163 ± 1
9.25	422 ± 11	283 ± 6	213 ± 3	153 ± 1
9.75	418 ± 12	261 ± 6	201 ± 3	144 ± 1
10.5	388 ± 12	237 ± 6	187 ± 3	130 ± 1
11.5	359 ± 12	255 ± 8	167 ± 3	114 ± 1
12.5	324 ± 13	209 ± 7	150 ± 3	104 ± 1
13.5	282 ± 12	195 ± 6	135 ± 3	94 ± 1
14.5	272 ± 12	186 ± 7	136 ± 3	85 ± 1
15.5	262 ± 13	171 ± 6	131 ± 3	79 ± 1
16.5	275 ± 14	155 ± 6	122 ± 3	75 ± 1
17.5	251 ± 12	146 ± 6	120 ± 3	73 ± 1
18.5	228 ± 10	149 ± 5	109 ± 3	69 ± 1
19.5	222 ± 10	150 ± 6	102 ± 3	69 ± 1
21	203 ± 9	142 ± 5	95 ± 3	67 ± 1
23	210 ± 9	124 ± 5	90 ± 3	62 ± 1
25	208 ± 10	117 ± 5	80 ± 3	60 ± 1
27	180 ± 9	112 ± 4	84 ± 3	58 ± 1
29	173 ± 9	106 ± 5	78 ± 3	58 ± 2
31	168 ± 9	105 ± 5	76 ± 3	59 ± 2
33	138 ± 9	112 ± 6	74 ± 3	54 ± 2
35	139 ± 10	101 ± 6	77 ± 3	49 ± 1
37	163 ± 11	98 ± 4	82 ± 3	47 ± 1
39	173 ± 13	98 ± 4	66 ± 3	46 ± 2
42.5	142 ± 12	86 ± 4	66 ± 2	47 ± 2
47.5	153 ± 15	78 ± 6	71 ± 2	45 ± 2
52.5	172 ± 24	72 ± 7	68 ± 5	40 ± 2
57.5		82 ± 8	64 ± 5	44 ± 5
62.5		88 ± 9	63 ± 4	52 ± 2
67.5		99 ± 11	75 ± 6	50 ± 3
72.5		134 ± 20	72 ± 5	62 ± 3
77.5			71 ± 10	57 ± 3
82.5			73 ± 9	75 ± 7
87.5				65 ± 5
92.5				55 ± 12

TABLE VII. $d^2\sigma/dtdM^2$ in μb/GeV^4 at $s = 741$ GeV^2.

M^2 (GeV^2) \ T (MeV) / t [(GeV/c)^2]	19 −0.036	40 −0.075	70 −0.131	105 −0.197
−65				0 ± 5
−55				0 ± 2
−45				−1 ± 2
−35			0 ± 5	−1 ± 2
−25			−4 ± 3	1 ± 2
−15		−8 ± 7	−9 ± 4	5 ± 2
−9.5		−18 ± 8	−3 ± 5	7 ± 2
−8.5		−10 ± 8	8 ± 5	9 ± 2
−7.5		−7 ± 8	15 ± 5	11 ± 2
−6.5		−4 ± 8	7 ± 6	12 ± 2
−5.5	26 ± 78	−2 ± 8	−4 ± 5	20 ± 2
−4.5	9 ± 46	4 ± 8	12 ± 5	30 ± 2
−3.5	13 ± 37	4 ± 8	37 ± 5	50 ± 3
−2.5	21 ± 31	42 ± 7	66 ± 5	79 ± 3
−1.5	50 ± 23	82 ± 6	91 ± 6	117 ± 5
−0.875	83 ± 22	86 ± 6	104 ± 5	141 ± 7
−0.625	126 ± 22	78 ± 7	112 ± 6	154 ± 8
−0.375	156 ± 23	88 ± 8	117 ± 7	168 ± 10
−0.125	199 ± 25	104 ± 9	144 ± 7	179 ± 11
0.125	246 ± 29	155 ± 10	173 ± 8	186 ± 13
0.375	362 ± 33	203 ± 12	218 ± 9	188 ± 14
0.625	459 ± 38	330 ± 14	267 ± 10	203 ± 16
0.875	611 ± 43	461 ± 15	327 ± 11	207 ± 18
1.125	792 ± 38	580 ± 14	416 ± 10	222 ± 16
1.375	1088 ± 33	771 ± 12	472 ± 9	219 ± 14
1.625	1461 ± 29	969 ± 10	550 ± 8	225 ± 13
1.875	1873 ± 24	1114 ± 9	577 ± 7	231 ± 11
2.125	2202 ± 21	1242 ± 8	623 ± 7	231 ± 10
2.375	2270 ± 20	1343 ± 7	644 ± 6	233 ± 8
2.625	2189 ± 19	1347 ± 7	659 ± 5	237 ± 6
2.875	1996 ± 19	1306 ± 7	632 ± 5	236 ± 5
3.125	1790 ± 19	1220 ± 7	607 ± 5	243 ± 3
3.375	1585 ± 20	1121 ± 7	566 ± 4	241 ± 3
3.625	1409 ± 20	1003 ± 7	548 ± 4	207 ± 3
3.875	1264 ± 21	888 ± 7	535 ± 4	186 ± 2
4.25	1114 ± 21	772 ± 7	499 ± 4	183 ± 2
4.75	931 ± 22	631 ± 8	444 ± 5	186 ± 2
5.25	775 ± 26	540 ± 8	391 ± 5	183 ± 2
5.75	630 ± 28	463 ± 8	357 ± 5	181 ± 2
6.25	491 ± 26	428 ± 8	316 ± 5	190 ± 3
6.75	449 ± 25	395 ± 8	288 ± 5	183 ± 3
7.25	426 ± 22	347 ± 8	272 ± 5	176 ± 2
7.75	462 ± 22	308 ± 8	246 ± 5	164 ± 3
8.25	452 ± 19	280 ± 8	236 ± 5	156 ± 3
8.75	421 ± 19	258 ± 7	220 ± 5	147 ± 2
9.25	353 ± 19	257 ± 9	209 ± 5	144 ± 3
9.75	292 ± 21	232 ± 8	198 ± 5	139 ± 2
10.5	327 ± 22	208 ± 7	182 ± 5	132 ± 3
11.5	421 ± 22	213 ± 9	159 ± 5	115 ± 2
12.5	374 ± 25	210 ± 8	134 ± 5	96 ± 3
13.5	300 ± 25	197 ± 8	118 ± 5	86 ± 2
14.5	270 ± 20	183 ± 8	122 ± 5	79 ± 2
15.5	231 ± 18	162 ± 9	113 ± 5	75 ± 2
16.5	255 ± 20	153 ± 9	107 ± 5	70 ± 2
17.5	301 ± 21	128 ± 8	106 ± 5	65 ± 3
18.5	238 ± 22	118 ± 9	102 ± 5	67 ± 3
19.5	125 ± 24	111 ± 8	96 ± 5	66 ± 3
21	137 ± 18	126 ± 7	96 ± 5	64 ± 3

TABLE VII. (*Continued*)

M^2 (GeV^2) \ T (MeV) / t [(GeV/c)^2]	19 −0.036	40 −0.075	70 −0.131	105 −0.197
23	150 ± 19	137 ± 8	86 ± 5	56 ± 3
25	179 ± 20	139 ± 9	68 ± 5	49 ± 3
27	154 ± 17	94 ± 8	62 ± 4	48 ± 4
29	156 ± 17	81 ± 6	73 ± 5	42 ± 3
31	207 ± 17	84 ± 7	76 ± 5	40 ± 3
33	170 ± 17	140 ± 8	57 ± 6	44 ± 3
35	164 ± 16	109 ± 8	57 ± 5	48 ± 3
37	166 ± 17	64 ± 8	57 ± 5	43 ± 3
39	138 ± 17	81 ± 7	60 ± 5	40 ± 4
42.5	134 ± 14	80 ± 6	65 ± 5	39 ± 4
47.5	136 ± 17	50 ± 6	52 ± 5	36 ± 3
52.5	141 ± 24	61 ± 6	64 ± 4	42 ± 3
57.5	146 ± 29	66 ± 7	50 ± 5	31 ± 4
62.5	172 ± 36	94 ± 10	47 ± 5	32 ± 4
67.5		102 ± 12	87 ± 10	49 ± 6
72.5		116 ± 13	50 ± 8	41 ± 7
77.5		83 ± 15	72 ± 8	44 ± 7
82.5		88 ± 17	53 ± 10	47 ± 6
87.5		83 ± 19	30 ± 12	27 ± 6
92.5		88 ± 32	41 ± 12	11 ± 8
97.5			38 ± 12	29 ± 10
105			30 ± 12	29 ± 7
115			35 ± 23	14 ± 10

[1]M. L. Good and W. D. Walker, Phys. Rev. 120, 1857 (1960).

[2]C. E. DeTar *et al.*, Phys. Rev. Lett. 26, 675 (1971); D. Silverman and C.-I. Tan, Nuovo Cimento 2A, 489 (1971); and Phys. Rev. D 3, 991 (1971); N. F. Bali *et al.*, *ibid.* 3, 1167 (1971).

[3]U. Amaldi *et al.*, Phys. Lett. 44B, 112 (1973); S. R. Amendolia *et al.*, Phys. Lett. 44B, 119 (1973).

[4]A. S. Carrol *et al.*, Phys. Rev. Lett. 33, 928 (1974).

[5]A. Capella *et al.*, Phys. Rev. Lett. 31, 497 (1973).

[6]K. Loebinger, in *Proceedings of the XVII International Conference on High Energy Physics, London, 1974,* edited by J. R. Smith (Rutherford High Energy Laboratory, Didcot, Berkshire, England, 1975), p. I-71.

[7]E. Leader and U. Maor, Phys. Lett. 43B, 505 (1973); R. E. Hendrick *et al.*, Phys. Rev. D 11, 536 (1975).

[8]R. P. Feynman, private communication.

[9]J. Pumplin, Phys. Rev. D 8, 2899 (1973).

[10]R. D. Field and G. C. Fox, Nucl. Phys. B80, 367 (1974).

[11]S. Childress *et al.*, Phys. Rev. Lett. 32, 389 (1974).

[12]J. Lee-Franzini *et al.*, in *Proceedings of the International Conference on High Energy Instrumentation, Frascati, Italy*, 1973, edited by S. Stipcich (Laboratori Nazionali del Comitato Nazionale per l'Energia Nucleare, Frascati, Italy, 1973), p. 454.

[13]R. D. Schamberger, Jr. *et al.*, Phys. Rev. Lett. 34, 1121 (1975) and Ref. 11.

[14]P. Franzini *et al.*, in *Proceedings of the International Conference on High Energy Instrumentation, Frascati, Italy* 1973, edited by S. Stipcich (Laboratori Nazionali del Comitato Nazionale per l'Energia Nucleare, Frascati, Italy, 1973), pp. 505 and 627.

[15]S. Childress, Ph.D. thesis, Columbia University, Nevis Report No. 216, 1976 (unpublished).

[16]C. Ankenbrandt *et al.*, submitted to the XVIII International Conference on High Energy Physics, Tbilisi, 1976 (unpublished).

[17]G. Barbiellini *et al.*, Phys. Lett. 39B, 663 (1972); A. Bohm *et al.*, *ibid.* 49B, 491 (1974).

[18]M. G. Albrow *et al.*, Nucl. Phys. B54, 6 (1973); B51, 388 (1973); B72, 376 (1974); B108, 1 (1976).

[19]K. Abe *et al.*, Phys. Rev. Lett. 31, 1527 (1973); 31, 1530 (1973).

[20]D. S. Ayres *et al.*, Phys. Rev. Lett. 37, 1724 (1976).

[21]V. Bartenev *et al.*, Phys. Lett. 51B, 299 (1974); Y. Akimov *et al.*, Phys. Rev. Lett. 35, 766 (1975).

[22]See for example, J. W. Chapman *et al.*, Phys. Rev. Lett. 32, 257 (1974); S. J. Barish *et al.*, *ibid.* 31, 1080 (1973); or F. T. Dao *et al.*, Phys. Lett. 45B, 399 (1973).

[23]S. Childress *et al.*, Phys. Lett. 65B, 177 (1976).

[24]V. Bartenev, Phys. Rev. Lett. 31, 1088 (1973) and Ref. 7.

[25]R. D. Schamberger, Jr., Ph.D. thesis, SUNY at Stony Brook, 1976 (unpublished).

[26]R. L. Anderson *et al.*, Phys. Rev. Lett. 38, 880 (1977).

[27]P. Franzini, in Proceedings of the II International Conference on Nucleon-Nucleon Interactions, Vancouver, 1977, edited by D. Measday (AIP, New York, to be published).